INLAND FRESHWATER LENS FORMATION AND IMPLICATIONS UPON DUNE DEVELOPMENT AT WHITE SANDS NATIONAL PARK

by

STEFFFAN BECKER

(Under the Direction of Adam Milewski)

ABSTRACT

Given the ecological and societal implications of access to freshwater resources, the relevance of their exploration is highlighted in a world with a rapidly growing global population and shifting climate. Recent studies in White Sands National Park have shown groundwater salinity as a contributing mechanism controlling transitions from barchan dunes to parabolic dunes. Although it is known that plant population density influences the transition from barchan to parabolic dunes, there is still a lack of understanding on the role hydrogeology plays in this system. In this study, we implemented a multi-faceted approach utilizing remote sensing, field investigation, and geostatistical analysis to verify the existence of Inland Freshwater Lenses (IFLs) in White Sands National Park and explore the impact of groundwater chemistry upon dune stabilization and dune morphology. Results from this study support the existence of a larger regional dune field IFL and localized IFLs beneath individual dunes.

INDEX WORDS: hydrogeology; water resources; remote sensing; groundwater; dune morphology, dune field

INLAND FRESHWATER LENS FORMATION AND IMPLICATIONS UPON DUNE DEVELOPMENT AT WHITE SANDS NATIONAL PARK

by

STEFFAN BECKER

BS Environmental Science, Georgia College and State University, 2018

A Thesis Submitted to the Graduate Faculty of The University of Georgia in Partial Fulfillment of the Requirements for the Degree

MASTER OF SCIENCE

ATHENS, GEORGIA

2021

INLAND FRESHWATER LENS FORMATION AND IMPLICATIONS UPON DUNE DEVELOPMENT AT WHITE SANDS NATIONAL PARK

by

STEFFAN BECKER

Major Professor: Adam Milewski

Committee: Robert A. Craddock

Charlotte Garing

Electronic Version Approved:

Ron Walcott

Vice Provost for Graduate Education and Dean of the Graduate School

The University of Georgia

December 2021

DEDICATION

I dedicate this thesis to Neva, Elliot, Erwin, and Kate Becker, the people who made me the man I am today. I love you all more than any words or actions I can offer. Thank you for helping me get to where I am.

ACKNOWLEDGEMENTS

This study would not have been possible without the support and help of many people in both my professional and personal life. I want to give thanks and acknowledgement to both of my parents for their unrelenting support to pursue a career that fulfills me and the patience they have graced me with through my up and downs to find my way here. They are the reason I am the man I am today and their selflessness to make me feel forever supported reminds me day in and day out of everything I desire to be in this world. Next, I want to thank my advisor, Dr. Adam Milewski. Thank you for giving me the opportunity to progress as an academic and cutting through the uncertainty I had about my abilities to succeed in this field. You have taught me a lot, both as a student of geoscience and a student of life. Additionally, thank you Dr. Charlotte Garing for your generosity with your time and knowledge that got me through the hump of finalizing this project. I would also like to thank you Dr. Robert Craddock for your guidance and expertise throughout this process and willingness to assist whenever and how ever you could. Next, I want to thank the Water Resources and Remote Sensing Lab as a whole. You have all become people I consider dear friends and my success in this program would not have been possible without the positive and supporting environment you all helped create in this lab. Lastly, I would like to thank all the wonderful staff at White Sands National Park, specifically David Bustos and Patrick Martinez for their generosity with their time and resources.

TABLE OF CONTENTS

Page

LIST OF TABLES

Page

LIST OF FIGURES

Page

LIST OF EQUATIONS

Page

CHAPTER 1

INTRODUCTION

Water resources are of great significance from a societal and environmental perspective and are only increasing in demand and consumption with a rapidly growing global population and shifting climate. With nearly 30 percent of the Earth's land surface being classifiable as arid and nearly a billion people living in these zones (Malagnoux, 2007) it is crucial to advance our understanding of these systems to improve water resources management in arid environments for a sustainable future. Arid zones must consider water extra meticulously in order to sustain access due to limited recharge and seasonally varying sources. Not only is freshwater an invaluable resource in regard to human impact, but also as a component of terrestrial ecosystems virtually everywhere on earth (Knight *et al*., 2005; Soininen *et al*., 2015). The ecological reliance of fresh groundwater for many plant species and the neighboring towns makes White Sands an ideal study site for the investigation of Inland Freshwater Lenses (IFLs). In addition to the biologic importance of IFLs, understanding how and where they form may also provide better insight into dune field dynamics and morphology, not only Earth, but also on the surfaces of other planets who's subsurface hasn't really been described yet (Chavdarian and Sumner, 2006; Fenton *et al.,* 2017).

White Sands is the largest gypsum dune field in the world and encompasses roughly 400 km^2 of the Tularosa basin in Southern New Mexico. Gypsum is a sulfate mineral formed through evaporative processes and the chemical formula is $CaSO_4 \cdot 2H_2O$. The unique environment is enclosed within the boundaries of White Sands National Park (WSNP) and White Sands Missile

Range. The basin is topographically closed in between the San Andreas Mountains to the west and the Sacramento Mountains to the east and discharges to the south into the Hueco Basin at a slow flow rate. The slow flow rate and restricted discharge point enable the shallow saline groundwater table to exist as it does (McLean, 1970; Basabilvazo et al., 1994).

This shallow groundwater table is part of a complex hydrological system with limited inputs, including heavy seasonal rainfall, mountain runoff, and fluvial inflow from ephemeral streams (Allmendinger, 1971; Fryberger, 2001; Talon and Allen, 2014). The complex stratigraphy of the upper 60 m, which consists of interfingering of gypsum dominated playa deposits in between alluvial clay deposits (Talon and Allen, 2014) makes it hard to generalize hydrologic characteristics. This stratigraphy also limits vertical flow and separates the shallow groundwater table from much of the deeper aquifer systems where freshwater can be found in the far eastern parts of the basin 400-1200m deep (Huff, 2002; Huff, 2004; Talon and Allen, 2014).

The stratigraphy, which controls the hydrogeology, is intricate due to a reasonably well-represented wide range of units dating back to the Precambrian, as well as active tectonic settings on the eastern (Jarilla Fault) and western (San Andres Mtns Fault) edges of the dune field (Talon and Allen, 2014). The shallow layers and surface geology are dominated by quaternary deposits composed mainly of gypsumiferous sediments (Fryberger, 2001). The gypsum deposits are the results of chemical precipitation in which lacustrine deflation has occurred, leaving behind evaporites (Allmendinger, 1971; Szynkiewicz et al. 2010). The roughly 6500-year-old dune field is a result of the deflated Lake Otero and has shown to have a stabilized parabolic dune field for approximately the last 3500 years (Langford *et al.*, 2009). A plethora of studies have described unidirectional winds from the Southwest to Northeast that have been the main source

of sediment transport creating the dune field (McKee & Douglass, 1971; Fryberger et al., 1988; Frank & Kocurek, 1994; Reitz et al., 2010; Jerolmack et al., 2012).

The shallow saline water table contributes to the controls upon dune field stability and sand mobility in White Sands. Studies by Langford et al. (2009) reported that groundwater salinity is a primary mechanism controlling dune field transitions from active barchan dunes to stabilized parabolic dunes. According to the current paradigm, aeolian processes control the dune field transition via an Internal Boundary Layer (IBL)on the western edge of the dune field (Jerolmack et al. 2012). This causes sediment deposition/erosion to reach an equilibrium with the vegetation's growth rate once past a certain boundary (roughly midway through the dune field), at which point stabilization is reached due to plant colonization of the dunes and decreased sediment transport (Reitz et al., 2010; Jerolmack et al., 2012).

Although apparent at a regional scale (km^2), this model does not acknowledge the impact of hydrology upon dune development and vegetation growth/density that is seen at a localized scale (m^2). The focus of our study was determining the existence and distribution of IFLs in the White Sands dune field. Little is known about IFSs in White Sands,but understanding their context in this setting is importand for assessing their effects on local dune, and perhaps even regional, dune development. We believe we can significantly advance our understanding of the dynamics of dune field evolution by further investigating the location and formation of fresh groundwater within the transitional and stabilized section of the White Sands dune field. We hypothesize that the development of IFLs in White Sands and other dune fields can help stabilize dunes even in the presence of strong aeolian forces and a regional saline aquifer.

Our objectives are three-fold:

I. Verify the existence of inland freshwater lenses through the use of
    a. geospatial analysis of available Light Detection and Ranging (LIDAR), vegetation surveys, and geochemical data from the existing observation well network
    b. a field survey to verify preliminary analysis and obtain higher resolution data at localized scale
    c. analysis of spatial trends in soil moisture and vegetation health observed via remotes sensing imagery to identify surficial expression
II. Test if the presence of lower salinity groundwater propagates stabilization by
    a. using field and remote sensing data to make a linear regression comparing groundwater salinity against vegetation health
    b. using field and remote sensing data to make a linear regression comparing vegetation health against dune mobility
    c. using the two linear regressions to subsequently demonstrate the relationship of groundwater salinity to dune mobility
III. Exhibit the coupled control of groundwater salinity and aeolian processes upon dune stability by implementing a three-dimensional cluster analysis showing the defining variables of dunes on each axis using the data collected from the LIDAR analysis and field study

With these objectives in mind the approach is split into three prongs; a pre-field geospatial analysis to determine trends in dune field migration in relation to groundwater and vegetation variables (which will focus field efforts), a field study to verify findings and further expand upon trends, and post-field processing of field data in conjunction with remote sensing data to make inferences about dune field processes in relation to groundwater dynamics.

The following chapters of this thesis build a framework demonstrating the importance, relevance, and impact that this study can have. The second chapter entails a literature review of relevant studies about dune morphology, IFLs, and remote sensing approaches. It will help to

guide this study and build a compilation of supplementary information to understanding key concepts explored in this thesis. Chapter three further details the study site characteristics such as geologic history, hydrogeologic properties, and climatic trends. Chapter four includes a detailed explanation of the methodology used to reach each objective. Chapter five details the results of our findings. Chapter six discusses the impacts of these results. Lastly the final chapter summarizes keys results and discussion points, as well as direction for future studies.

CHAPTER 2

LITERATURE REVIEW

Understanding the different aspects of the transport/deposition and the morphology of dunes can give us insight into the controlling factors of a dune system here on earth and extra-terrestrial bodies within our solar system, such as Mars (Chavdarian and Sumner, 2006; Fenton *et al.,* 2017). With factors such as grain size, vegetation, soil moisture, soluble salts, crusting, and cohesion being relevant to the mobility of sediment in an aeolian dune system, parsing the dominant mechanisms can be difficult (Nickling and McKenna-Neuman, 1994; Scheidt *et al.*, 2010). There are five main aeolian dune forms recognized: barchan, linear, dome, star, and parabolic (USGS, 1997). The relationship between parabolic dunes and barchan dunes is a well-documented one with the absence or presence of vegetation being a key part of the transition from one form to the other (e.g., vegetation leading to stabilization and parabolic dunes) (Bagnold, 1941; Lockwood, 1995; Durán and Herrmann, 2006; Reitz *et al.*, 2010; Jerolmack *et al.*, 2012). Aeolian processes are also well understood to play a large role in dune field dynamics; however, it does not always account for localized implications (Bagnold, 1941; Jerolmack *et al.*, 2012). The hydrogeological perspective serves to explain these instances of localized abnormalities in regional trends of dune movement through the existence of inland freshwater lens (IFL) formation.

2.1 Inland Freshwater Lenses

IFL development has only been examined relatively recently when compared to the far more common global distribution of oceanic freshwater lenses. Laattoe *et al.* (2017) presented the classification of the identified IFLs to date and categorized the different types using four criteria: geologic setting, topography, recharge mechanisms, and groundwater -surface water interaction (2017). Of the fifteen identified IFLs mentioned in publications up to that point, there is limited data to describe the majority of them (Laattoe *et al.,* 2017). However, they appear ubiquitous and they have been discovered in Australia (Barret, 2002), Botswana (Bauer *et al*., 2006), Florida (Panday *et al.*, 1993), Kuwait (Kwarteng *et al.*, 2000; Milewski *et al.,* 2014), New Mexico (Langford *et al.*, 2009), Paraguay (Houben *et al.,* 2014), Pakistan (Asghar *et al.*, 2002), Turkmenistan (Kacimov and Obnosov, 2019) and Zambia (Chongo *eta al.*, 2015). In several instances the IFLs are known to be used by residents in the surrounding areas such as the Benjamín Aceval lens in Paraguay (Houben *et al.,* 2014), Raudatian lens in Kuwait (Kwarteng *et al.*, 2000; Milewski *et al.,* 2014) and the Shashe River Valley lens in Botswana (Bauer *et al*., 2006). These communities demonstrate the potential for IFLs to meet a quickly expanding global population and increasing demand for freshwater resources.

Of those mentioned above two formation settings hold a more significant relevance to this study: topographical lows (drainage depression) or topographic highs (mound). Although forming settings exist, these demonstrate the most commonly found in arid regions. The application of physical models, numerical modeling, hydrogeological tests, chemical analysis, geophysical surveying, and drilling have been used to fill in gaps of our understanding around IFLs. Rotz and Milewski‘s (2019) physical model demonstrated the degradation of an IFL without sufficient recharge using a physical tank model in conditions mimicking a depressional

formation setting as seen in **Figure 1**. This model helped create the framework around this type of IFLs geometry, with which they were able to numerically model and incorporate more variables representative of a real system (Rotz, Milewski, and Rasmussen, 2020).

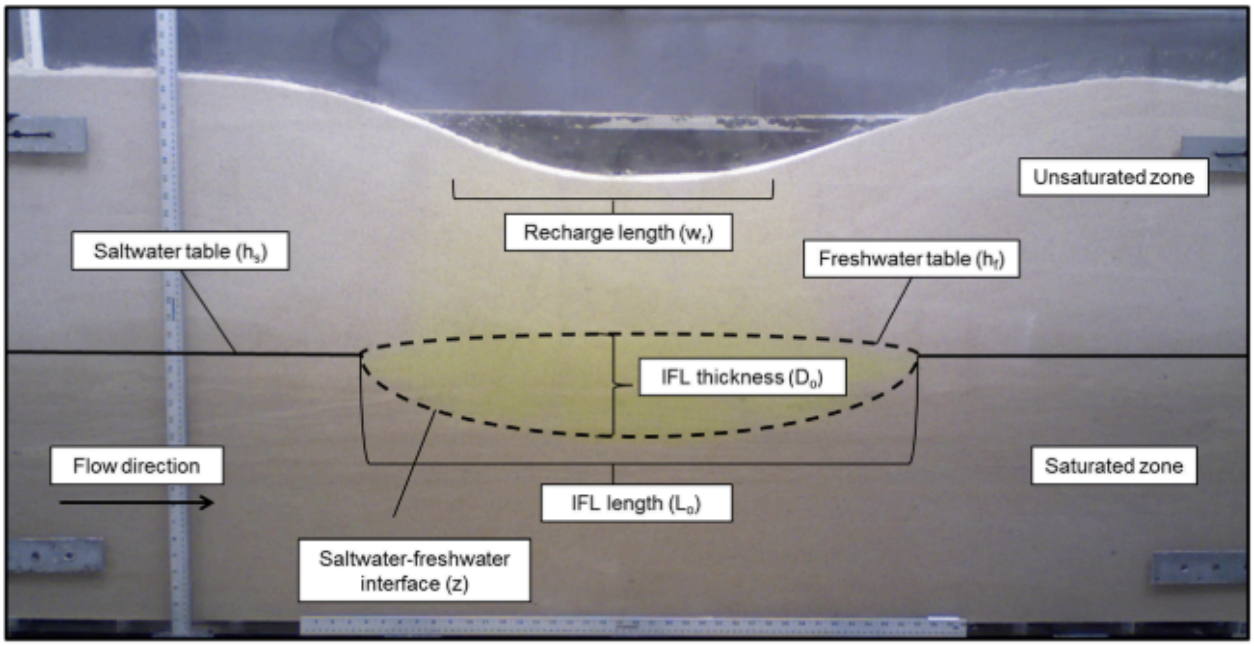

Figure 1. Physical model displaying the geometry of an IFL in a topographic depression setting. Adapted from Rotz and Milewski (2019).

Topographic mounding has been conceptually modeled based on the Karakum desert of Turkmenistan and the conditions are described through a set of detailed equations (Kacimov and Obnosov, 2019) as seen in Error! Reference source not found.. This type of lens fits perfectly in the structural understanding of dune water retention that is a result of sand's poor thermal conductivity and thus high capacity for water retention due to an even temperature distribution through the majority of the dune (Bagnold, 1941). IFL formation is dependent upon sediment with a high infiltration rate, intense sporadic rainfall events, and topographic mounding or a depression, atop of saline groundwater (Laattoe *et al.,* 2017; Rotz and Milewski, 2019; Kacimov and Obnosov, 2019).

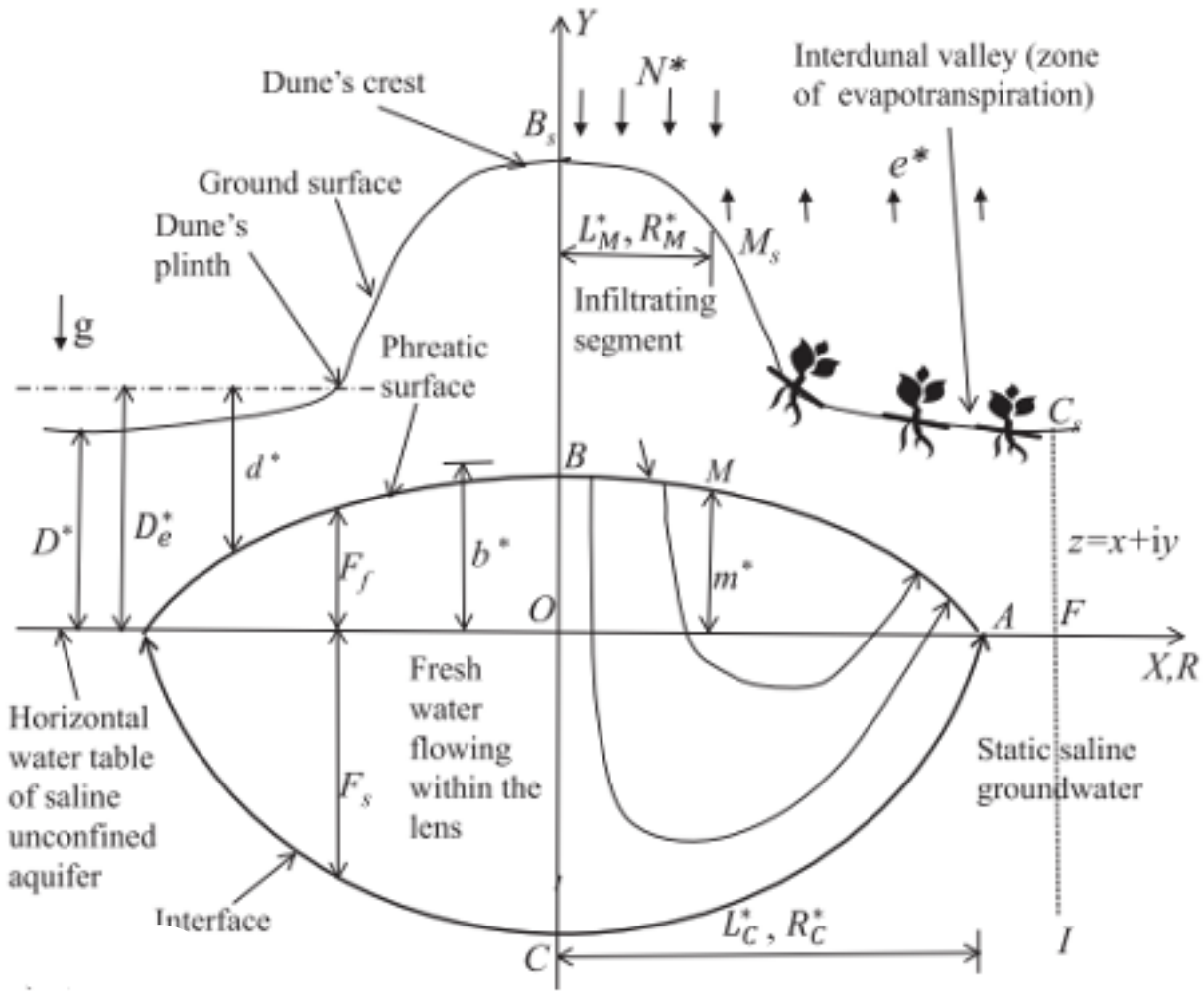

Figure 2. Conceptual Model displaying IFL under a topographic mound. Based off the dune field in the Karakum Desert in Turkmenistan. Adapted from Kacimov and Obnosov (2019).

Thus, the setting needed for the development of IFLs is ideal within WSNP given the presence of a shallow saline water table (<3m throughout most of the park), a monsoon season (early July – late Sept.), and a dune field, creating both mounds and interdune swales. White Sands is a wet aeolian system, with the accumulation surface confined by the height of the water table (Fryberger *et al.*, 1988; Kocurek *et al.,* 2007). The regional water table is a shallow (<1m - 3m) saline system, with flow trending NE to SW (Talon and Allen, 2014), which is the opposite of the prevailing winds that are responsible for dune migration patterns (Kocurek *et al.,* 2007). The San Andreas Mountains and the Sacramento Mountains bound the Tularosa basin to the

West and East respectively, concentrating discharge toward the south in the Hueco Basin at a slow rate of flow. The shallow groundwater table is a result of the slow flow rate and bounded discharge point (McLean, 1970; Basabilvazo *et al*., 1994).

Grain size distribution and sediment supply analyses have been performed by several groups and show that gypsum's ready availability, easier erosion and greater mobility for transport allow for it dominate the make-up of the area over other minerals (Chavdarian and Sumner, 2006; Jerolmack *et al.*, 2011; Fenton *et al.,* 2017). The stratigraphy of the upper 60 m makes it hard to generalize hydrologic characteristics due to interfingering of gypsum dominated playa deposits in between alluvial clay deposits (Talon & Allen, 2014). The dynamic between the saline groundwater and gypsum's propensity for dissolution complicates the recognizability of freshwater due to the nature of salts to raise the conductivity of water. For use in the field, most probes derive salinity values using a ratio applied to the conductivity measurement picked up from running a current between two submerged electrodes (Slinger and Tension, 2007). Chemical analyses of ion concentrations give important information that can give insight as to the origins of the water as well as a clearer picture of the degree of dissolution.

In studies analyzing hydrogeology and dune systems the incorporation of remote sensing techniques has allowed for the focused efforts of in situ investigation methods, but also comprehensive understanding of large scale or regional trends surrounding multiple variables. The capability of scientists to use these techniques is further compounded upon by the availability of data sets to the public for free at relatively high resolutions. Advancements in drone technology and accessibility also make even higher resolution data possible for studies focusing on more small-scale variables and localized processes.

2.2 Groundwater Quality and Vegetation

The chemical, biological and physical processes that govern water quality take on a variety of combinations that impact the fate of water in a system. Concentrations of Sodium Chloride (NaCl) have long been known to be toxic to the health of vegetation, having been used since 3000 BC to destroy crop fields in enemy lands during times of war (Brod, 1993; Blomqvist, 1998). With the vast majority of this planet's water being saline, it is vital to understand salt transport mechanisms. NaCl is readily dissolved in water, allowing ions to move freely in solution, with the Cl ion being highly mobile and thus easily transported through groundwater (Blomqvist, 1998). The transport of the Na ion is often held back due to its ability to take part in cation-exchange processes that result in the release of calcium (Ca) and magnesium (Mg) (Cates *et al*, 1996). It has been observed that in areas where de-icing regularly takes place on roadways throughout the year that the spread of salinized water has negative effects on the vegetation up to several hundred meters beyond the zone of spray and away from the flow paths of run off (Blomqvist, 1998), demonstrating exactly how mobile salt ions are in groundwater.

Although many species of plants have evolved a degree of salt tolerance, it is evident that this does not make the plant excel. Plants with salt tolerances can withstand salinity up to a certain threshold (depending upon the species), but they do better under conditions where this stressor is limited, thus allowing for the growth of greater biomass both above and below the ground surface (He *et al.*, 2017). In addition to the typical compound that comes to mind for salt, gypsum ($CaSO_4$) is a chemical salt and can impact plant health as well. Although toxicity for plants from the presence of gypsum is not typically as threatening, it does have the ability to build up within the cytoplasm of the cells and inhibit important processes that regulates stomatal

aperture in response to changes in carbon dioxide (CO_2), temperature, and water availability (Borer *et al.*, 2012).

Much of the vegetation in White Sands has developed significant adaptations to the harsh environmental conditions. Multiple plants including *Poliomintha incana* (desert rosemary mint) and *Tamarix gallica* (salt cedar) have adaptations to manage the salinity and Ca buildup utilizing salt exudation through foliar[1] salt glands (Borer *et al.*, 2012). Although this does not make the plant impervious to overload of certain constituents, it does help relegate the impacts of these chemicals building up within the organism.

A comprehensive understanding of the solutes present within the water table can give insight as to the effect they are having on vegetation health. This can be done cost effectively and precisely through the use of ion chromatography. Ion chromatography is an automated separation technique that uses an anion exchange column to pass anions through resin and separate them based on species and size by measuring retention time within the resin (Bauer and Gluhak, 2019; Bruckner, 2021). The utilization of ion chromatography in conjunction with an understanding of plant chemical processes and remotes sensing data on regional trends in vegetation health can give insight about the impact of groundwater chemistry on a system that is dependent upon vegetation for geomorphologic processes.

2.3 Remote Sensing and Geographic Information Systems

Applications for remote sensing (RS) in the geosciences have been rapidly expanding since the 1980's with advancements in sensors and the increasing availability of data. The integration of RS processing software (e.g. ENVI) with geographic information systems (GIS) (e.g. ArcGIS) has expanded the capabilities of implementing statistical analyses quicker and

[1] *Of or relating to the structure of the leaf.*

easier. The utilization of satellite observations in conjunction with a GIS database have been applied in studies performing vegetation health mapping (Lee and Yeh, 2009), lithologic mapping (Elewa and Qaddah, 2011), drainage pattern delineation (Kwarteng *et al.*, 2000; Elewa and Qaddah, 2011; Milewski *et al.*,2014), IFL formation potential mapping (Kwarteng *et al.*, 2000; Milewski *et al.*,2014), and dune field evolution tracking (Dong, 2015; Rodríguez-Santalla *et al.*, 2021) amongst other objectives.

Kwarteng *et al.,* (2000) used aerial Landsat Thematic Mapper (TM), aerial photographs, and digital elevation models (DEM) to map paleo-drainage patterns, playas, large topographic depressions, and catchment areas, which are important features for the formation of IFLs. Since the advancement of computing power and data availability Milewski *et al.*, 2014, have validated and expanded upon these finding through the incorporation of an extensive database with more recent satellite imagery amongst other updates. Milewski *et al.'s* (2014) study shows how the advancements in technology and data availability have increased scientist capacity to cover large swaths of land to reveal insights about the effects of complex patterns.

Using LIDAR the creation of very high resolution DEM's have allowed for detailed tracking of dune processes that are otherwise extremely time consuming to record from the surface. LIDAR utilizes a laser to emit pulses of light and calculates the time of return to define the distance and create a point cloud. With features like dunes and the variability of their morphology, even within one type (e.g., barchan), the sampling of many occurrences in a scene makes for more robust findings. Dong (2015) created an automated dune migration add-in for ArcGIS that uses a temporal range of LIDAR data to track the movement of multiple dunes within a scene and determine annual movement rates. Using this data, inferences can be made

about the wind speeds and frequency's effect and the localized impact upon these processes via the use of knowledge about spatial variability (e.g. plant density).

When considering the mapping of vegetation via remote sensing considerations must be made about the data's spectral, spatial, radioactive, and temporal characteristics in order to achieve the extraction of the desired information (Xie *et al.*, 2008). The use of band math to create an index for variables commonly needed, like the normalized difference vegetation index (NDVI), can give spectral signatures that specifically identify a desired output. The NDVI is often used to map swaths of vegetation health due the strong reflectance and absorption from plants in the near infrared and red wavelength (Xie *et al.*, 2008; Lee and Yeh, 2015). Tracking the stress upon plants in highly salinized areas can be indicated through this method and give insight about the impact of zones with fresher vs saline water.

Thermal remote sensing utilizes the thermal infrared wavelengths emitted from surfaces of objects to make inferences about the state of said object. In a paper by Scheidt *et al.*, (2010) the relationship of Land Surface Temperature (LST) and apparent thermal inertia is used to model, soil moisture, actual thermal inertia, and the wind threshold velocity ratio via Advanced Spaceborne Thermal Emission and Reflection (ASTER). This information provided insight as to the stabilizing effects of precipitation and the water table upon sediment availability for transport and predicting dust storms as a consequence. The Soil Moisture Index is often modeled via the relationship between LST and vegetation health (often determined via the NDVI or other similar indicies) (Parida *et al.*, 2013; Saha *et al.*, 2018).

CHAPTER 3

STUDY SITE

3.1 Physiographic Setting

White Sands is the largest gypsum dune field in the world and encompasses roughly 400 km^2 of the Tularosa basin in Southern New Mexico as can be seen in **Figure 3**. The unique environment is shared between the boundaries of WSNP and White Sands Missile Range. The north-south trending valley of the Tularosa basin is topographically enclosed in between the San Andreas Mountains to the west and the Sacramento Mountains to the east. The topography focuses out flow to the south into the Hueco Basin. Due to the limited outlet point and subtle slope, the shallow groundwater table is capable of existing as it does (McLean, 1970; Basabilvazo *et al.,* 1994). The shallow groundwater table has become the limiting factor of deflation for the dune field that has developed over the last 7,000 years (Kocurek et al., 2007). The sediment supply of the dune field comes from the evaporite minerals formed from the evaporation of Pleistocene-Lake Otero (Fryberger, 2001) that was fed by mountain runoff water rich in dissolved evaporites. The lake began receding at the end of the last glacial maximum as temperatures were rising and aridity increased, resulting in extensive gypsum-rich playa deposits forming (Fryberger, 2001).

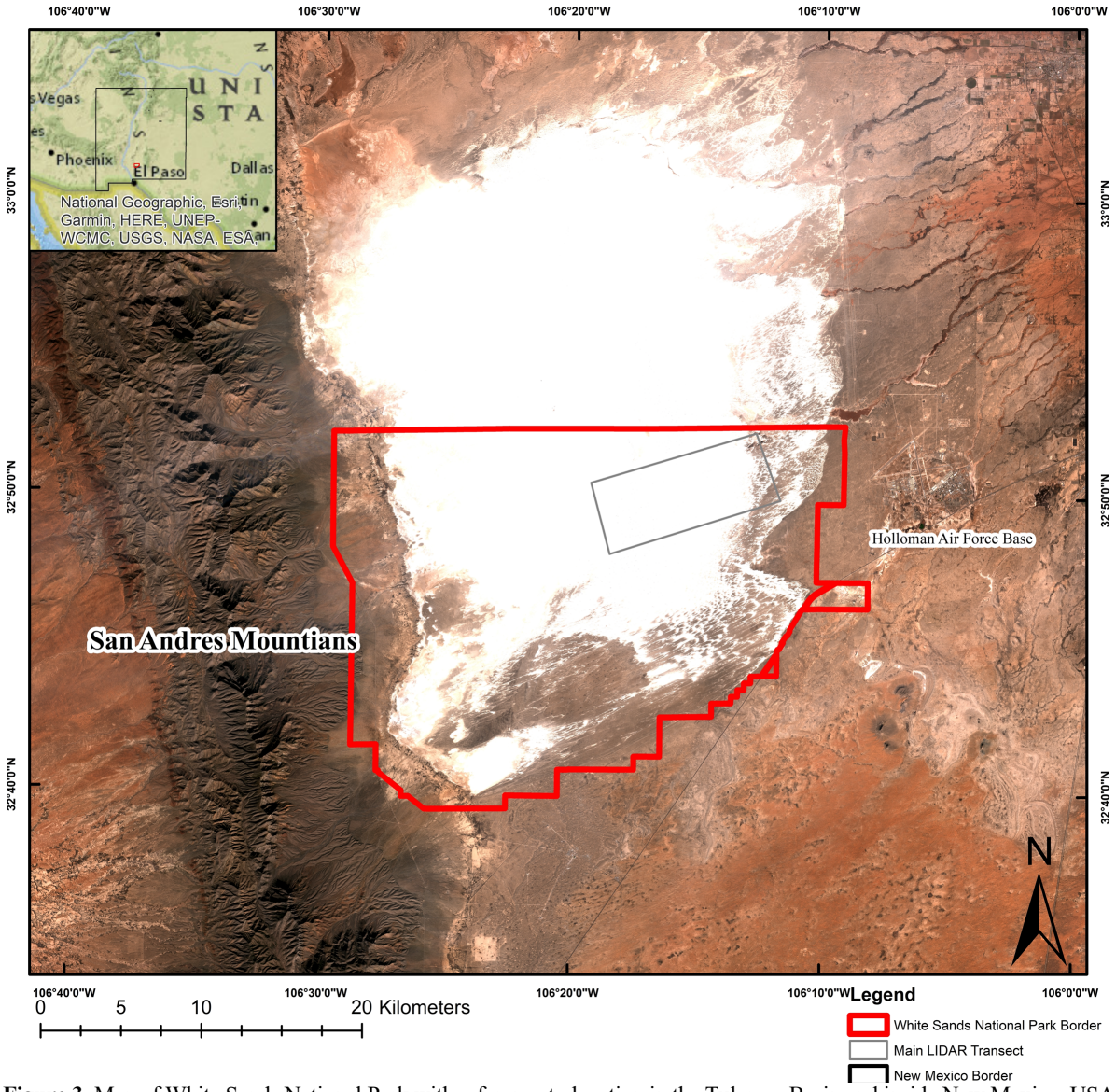

Figure 3. Map of White Sands National Park with reference to location in the Tularosa Basin and inside New Mexico, USA.

The basin floor is composed of alluvial-fan playa deposits of evaporite minerals including primarily gypsum, but also halite and other salt minerals in smaller concentrations (mirabilite, thenardite, etc.). The gypsum rich evaporite beds have formed the dune field through aeolian processes that transported the vast deposits from the area known as the Alkali flats over the last 7,000 years. It is from these deposits that distinct formational areas of active and inactive dunes with unique morphology, interdunes, and sand sheets have become the dune field observed today (Fryberger, 2001; Bourret, 2015).

3.2 Geologic Setting

The Tularosa Basin marks the beginning of a southward trending increase in the widening of the Rio Grande Rift (Adams and Keller, 1994). Approaching this region, the crust thins in the southern part of the rift zone (Adams and Keller, 1994). Being a small component of a larger physiographic north-south trending chain of rift valleys, the Tularosa Basin contains a complex tectonic setting complicated by the lack of visible features due to the basin fill deposits overlaying surface expressions. For this reason, the exact location of the Jarilla fault on the eastern edge of the dune field is not precisely known. Its mapping was attempted using shallow geophysical methods, however, with little success owing to the complex nature of the fault zone near the surface (Reynolds, 2012; Talon and Allen, 2014). The map below shows the extent of where the intrabasin fault is thought to exist in the basin as well as other major geologic features **(Figure 4**).

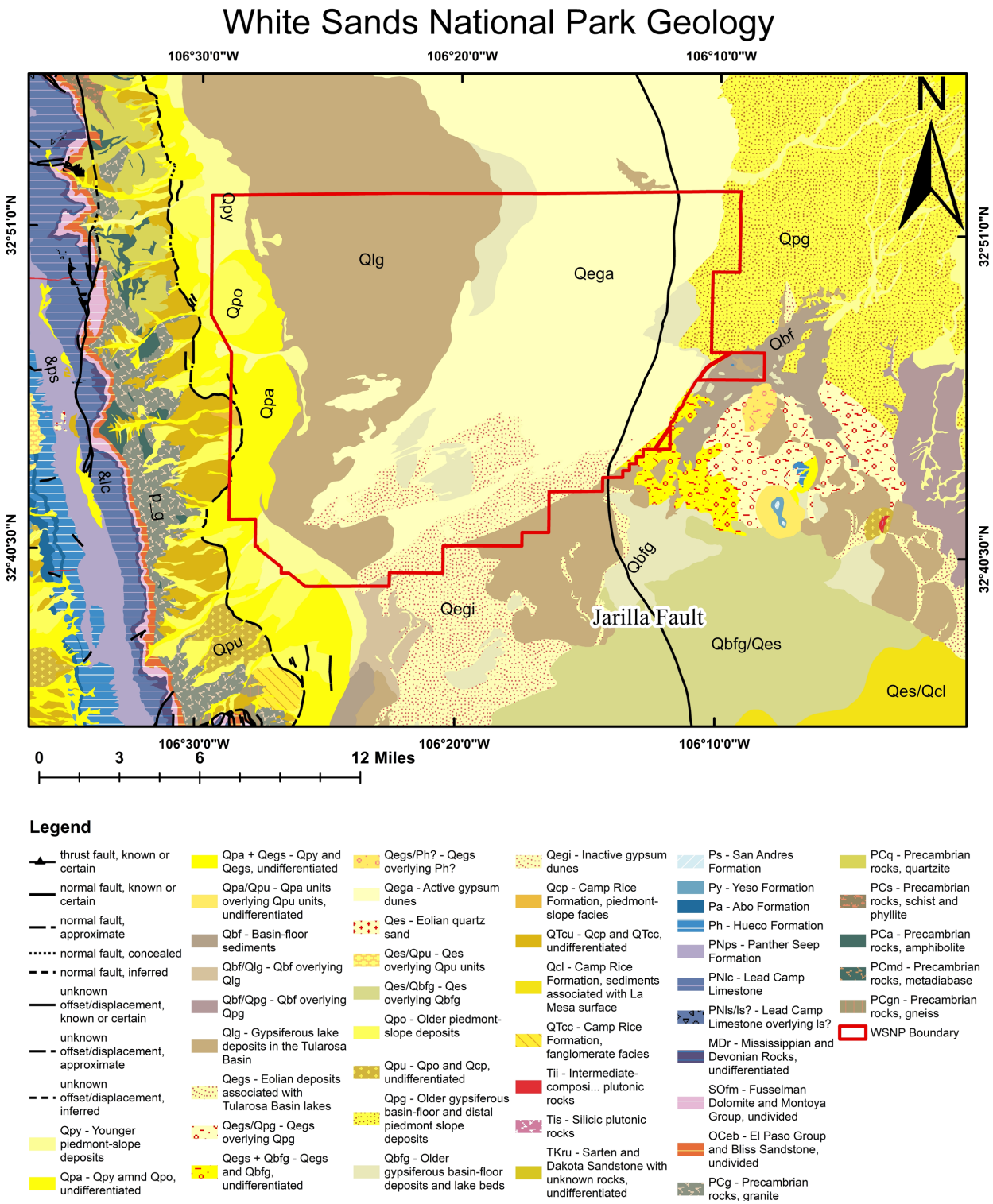

Figure 4. Geologic map of surficial units and location of major faults in and surrounding WSNP. Data from provided by WSNP staff.

The rift began forming roughly 35 Mya at rapid pace with low angle faulting along both the Sacramento and San Andreas Mountains (Keller *et al.,* 1990; Huff, 2005). The region's rapid tectonic and magmatic activity decreased from 18 Mya to 10 Mya. From 10 Mya to present, extension has increased, resulting in high angle normal faulting (Keller *et al.,* 1990). Exposures of Precambrian granite and metamorphic rocks are evident along the base of both flanking mountain ranges; however, it is of greater proportion than those seen along the eastern edge of the San Andreas Mountains. The surrounding mountain ranges are capped mostly with Paleozoic sedimentary rocks, dipping to the east in the eastern range and dipping toward the west on the western range (Talon and Allen, 2014). At the northeastern perimeter of the basin the tallest mountain, Sierra Blanca, shows evidence of tertiary age igneous activity with Oligocene volcanic rocks and varied igneous intrusions throughout the tertiary period (Talon and Allen, 2014).

Much of the gypsum-playa deposits formed from alluvial and fluvial processes are a result of transport of material from the marine deposited Yeso formation of the Permian (Huff, 2002; Szynkiewicz *et al.,* 2009). Due to the lack of surface outlets in the basin, much of the mountain runoff was channeled into Pleistocene Lake Otero (now Lake Lucero), resulting in the high concentrations of salt type minerals such as gypsum, halite, and others (Szynkiewicz *et al.,* 2009). Lake Otero encompassed nearly 2000 km^2 of the Tularosa Basin from 45 kya to 15.5 kya and exists as remnant features of the ancient lake, now known as Lake Lucero and the Alkali Flats. Since the end of the last glacial maximum Lake Otero has evaporated leaving behind the gypsum-playa deposits (Kocurek *et al.,*2007; Langford *et al.,* 2009). Over the last 7,000 years the increased aridity of the region has allowed for a prevailing southwestern wind to transport and deposit material from the gypsum rich Alkali Flats into the dune field that makes up White Sands (Kocurek *et al.,*2007; Langford *et al.,* 2009).

3.3 Hydrogeologic Setting

Quaternary basin-fill deposits are the medium that most of the useable regional aquifer storage resides in within the basin. The remaining components of groundwater storage in the deeper basin fill and bedrock are largely inaccessible or irrelevant to use, with salinity levels being that of brine (McLean, 1970). The thickness of aquifer units varies in thickness significantly within the basin, ranging from 30 m to 250 m, with depth to water ranging from 20 m to 90 m (McLean, 1970). However, the depth to water for the shallow groundwater table underlying the dune field is typically within 0 to 2 m. This part of the basin not only has the shallowest depth to water but also some of the lowest elevations of the water table, as can be seen in **Figure 5**. The majority of water entering the dune field system comes from lateral flow of the greater Tularosa Basin, with vertical flow being limited by the interfingering of clay deposits and very miniscule amounts of precipitation (Huff, 2005; Talon and Allen, 2014).

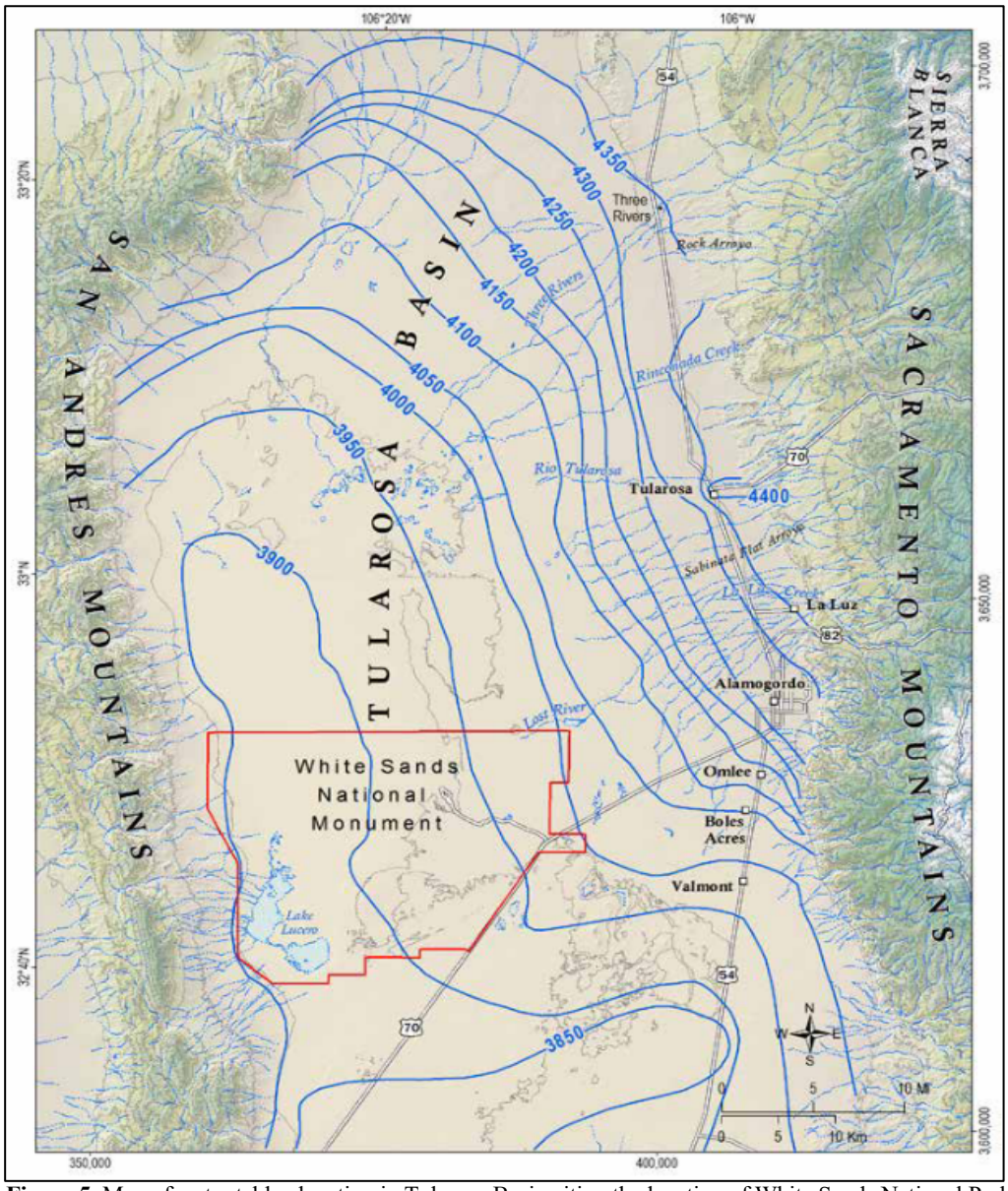

Figure 5. Map of water table elevation in Tularosa Basin citing the location of White Sands National Park. Adapted from Talon and Allen (2014).

Salinity has been shown to vary from the eastern edge to western of the dune field with increasing salinity moving toward the Alkali Flat and Lake Lucero (Fryberger 2001; Langford *et al.,* 2009). The groundwater table slightly mimics the topography, with elevation decreasing in the same direction, however there is more significant depth to water table in the east that decreases moving westward (Fryberger 2001; Langford *et al.,* 2009), with the exception of several surficial springs in the far north-western edge of the dune field near the ephemeral Lost River. The Lost River is also an exception to WSNP regional groundwater trends in salinity, with

groundwater underneath the riverbed being extremely saline and likely fed from the Tularosa basin's regional aquifer (Talon and Allen, 2014). Additionally, Garton Pond is a remnant marsh to the southeast of the WSNP visitor center that was created from the uncontrolled artesian flow of deep groundwater containing brine-like salinities (McLean, 1970; Talon and Allen, 2014). It has since depressurized and stopped flowing and only seasonally ponds during precipitation events.

3.4 Climatic Setting

The aridity of the Tularosa Basin's climate has continually increased since the last glacial maximum, turning the environment of a once cooler and wetter regional climate into the arid to semi-arid desert it exists as now (Metcalfe *et al.,* 2000). Projections of future climate conditions in the Southwestern United States show that the region will continue to increase in aridity (Seager *et al.,* 2007) and may heavily increase evapotranspiration of the limited surface water sources, while decreasing recharge to the groundwater table from precipitation. This has the potential to heavily impact the flora and fauna that have adapted to this environment, as well the stability of the dune field through the loss of groundwater and vegetation stabilization.

Precipitation is the main source of regional recharge to the Tularosa basin, however groundwater underlying the dune field largely comes from lateral flow, with precipitation making up <10% of input into the shallow groundwater table (Allmendinger, 1971; Huff, 2005; Talon and Allen, 2014). Annual precipitation to the dune field is ~20 cm/yr during the monsoon season that last from July to September (Allmendinger, 1971; Kellerlyn, 2012; Talon and Allen, 2014). Due to the heat and mostly barren landscape within the dune field much of this water is lost to evapotranspiration at a higher rate. Losses near Lake Lucero have been recorded as much as 270 cm/ year in contrast with those recorded at Holloman Air Force base being closer to 120

cm/yr (Bourret, 2015). The prevailing wind goes from southwest to northeast throughout the majority of the year, but seasonal variability does occur as can be seen in the rose diagrams adapted from Kocurek et al. (2007) **Figure 6**.

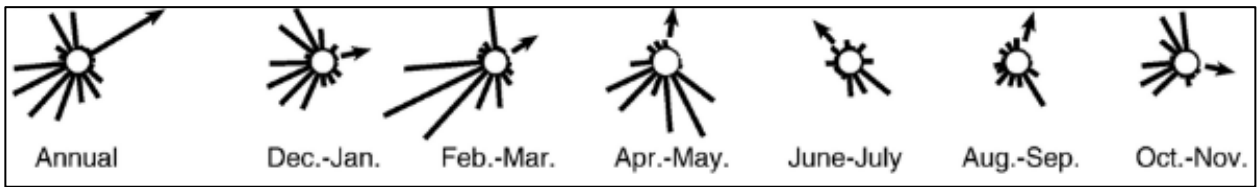

Figure 6. Rose diagrams of wind regime taken from data recorded at Holloman Airforce base. Adapted from Kocurek *et al.* (2007).

3.5 Site Specific Available Data

White Sands National Park contains a limited system of wells equipped within the park that are equipped with transducers that record variables including conductivity, salinity, soil moisture, soil temperature, and precipitation. The wells were installed on dates between 2018 and 2019. They take measurement every fifteen minutes. There are seven wells total, of which one is also a weather station. There are also several additional weather stations measuring solely meteorological characteristics. The wells and weather stations can be seen below in **Figure 7**.

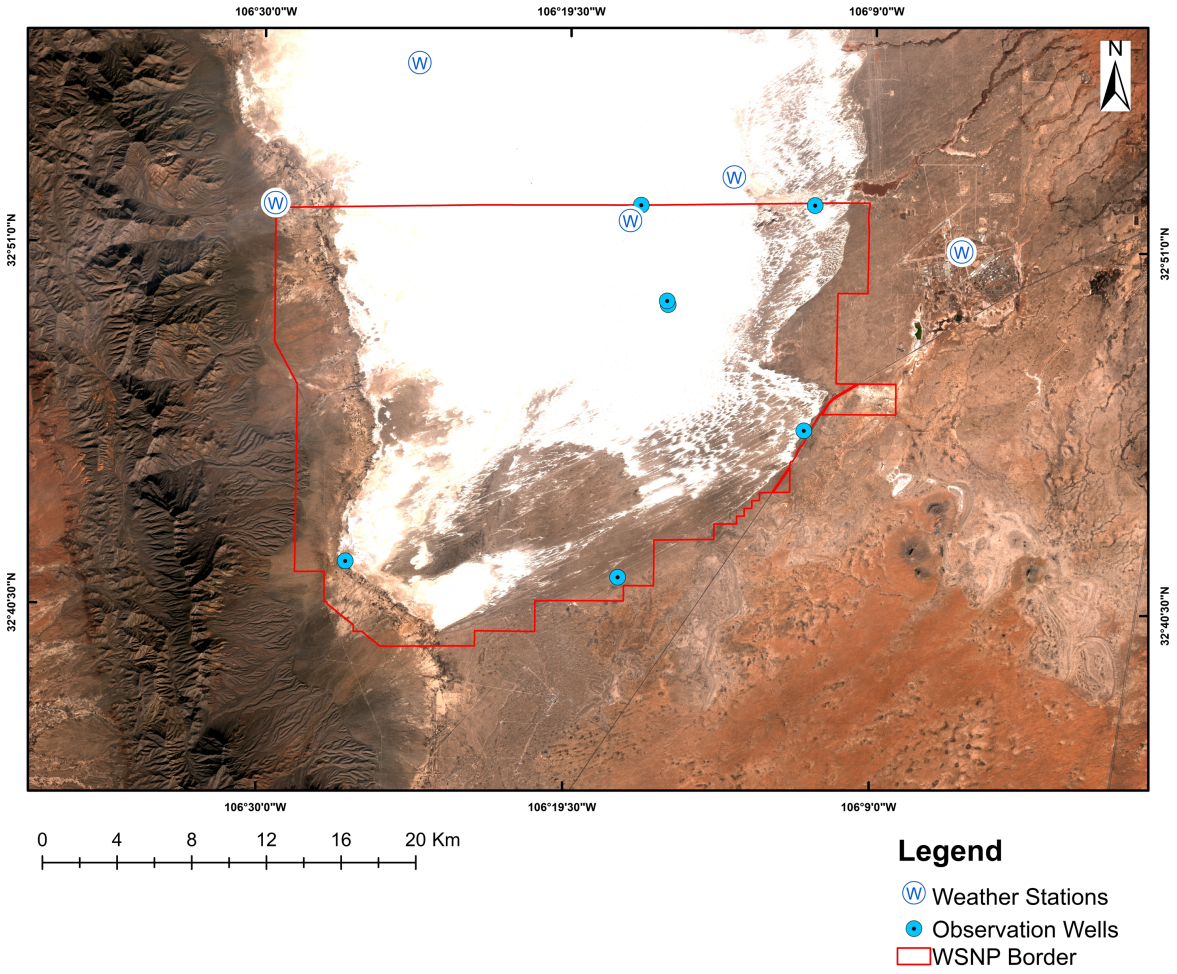

Figure 7. Map detailing locations of WSNP well and weather station network. Data for sites available through WSNP data repository portal.

Via the NPS data repository we were able to access shapefiles detailing the findings of a 2016 vegetation classification performed in and around the park. The classification details the dominating land cover, such as different vegetation types/combinations, roads, and barren land. The vegetation classification map can be seen below in **Figure 8**. The NPS repository also included a geodatabase and the shapefiles needed to create the geologic map seen in **Figure 4.**

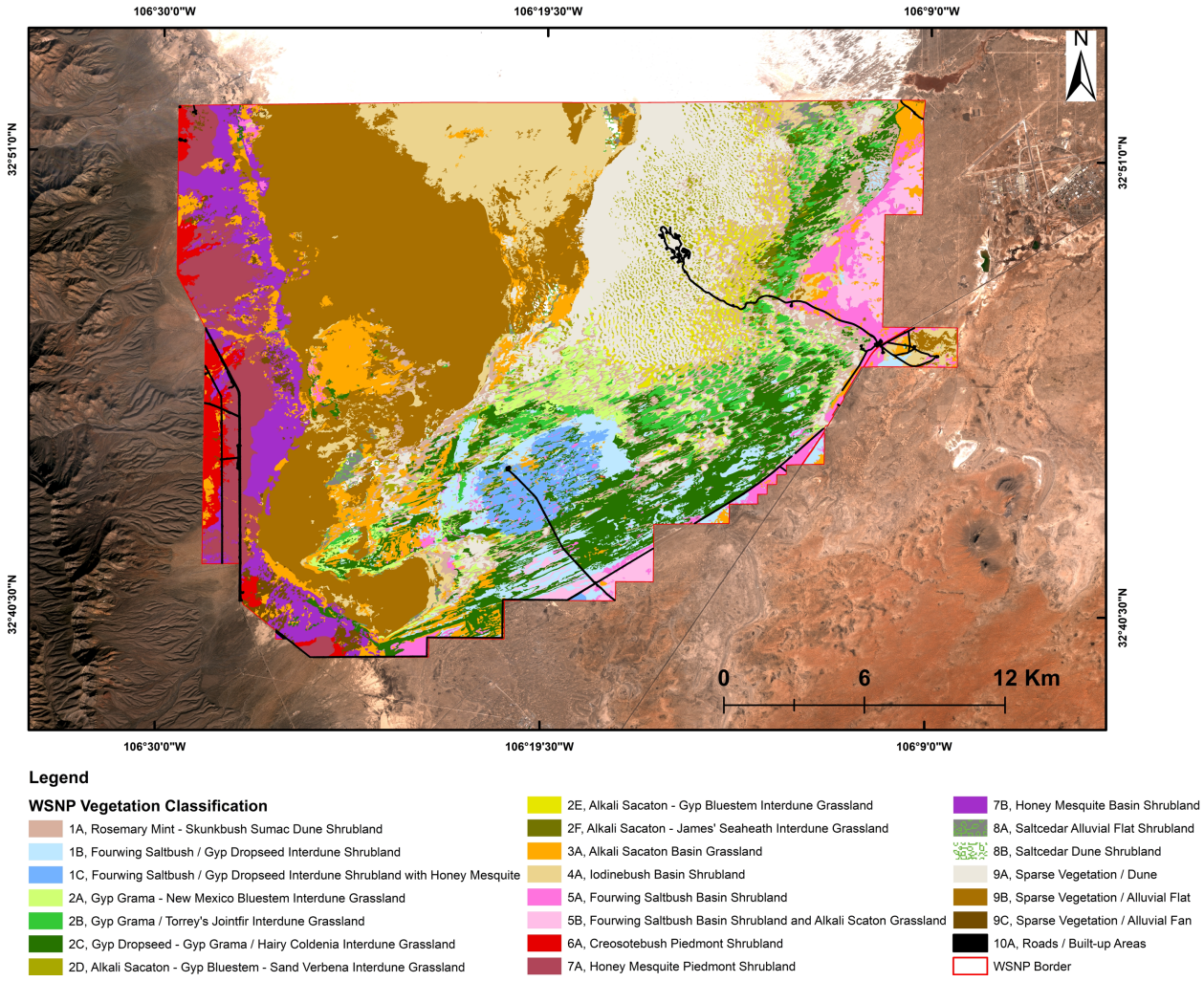

Figure 8. Vegetation classification map of the predominant vegetation types throughout WSNP from 2016 survey. Data from provided by NPS data repository.

Georeferenced and proofed LIDAR surveys were made available from the WSNP Resource Manager for June 2007, June 2008, January 2009, June 2010, and January 2016. All surveys were of a 39km^2 transect in the area known as the Heart of the Dunes, except 2016. This survey covered the same transect plus additional area reaching the northern extent of the park's boundaries and farthest seasonal extent of the ephemeral Lost River. The 2016 survey spatial resolution is .25m x .25m x .04 m. All other surveys were 1m x 1m x .04 m. LIDAR was georeferenced using 135 non-moving points within the park including park structures and pedestal dunes. LIDAR surveys can be seen below in **Figure 9**.

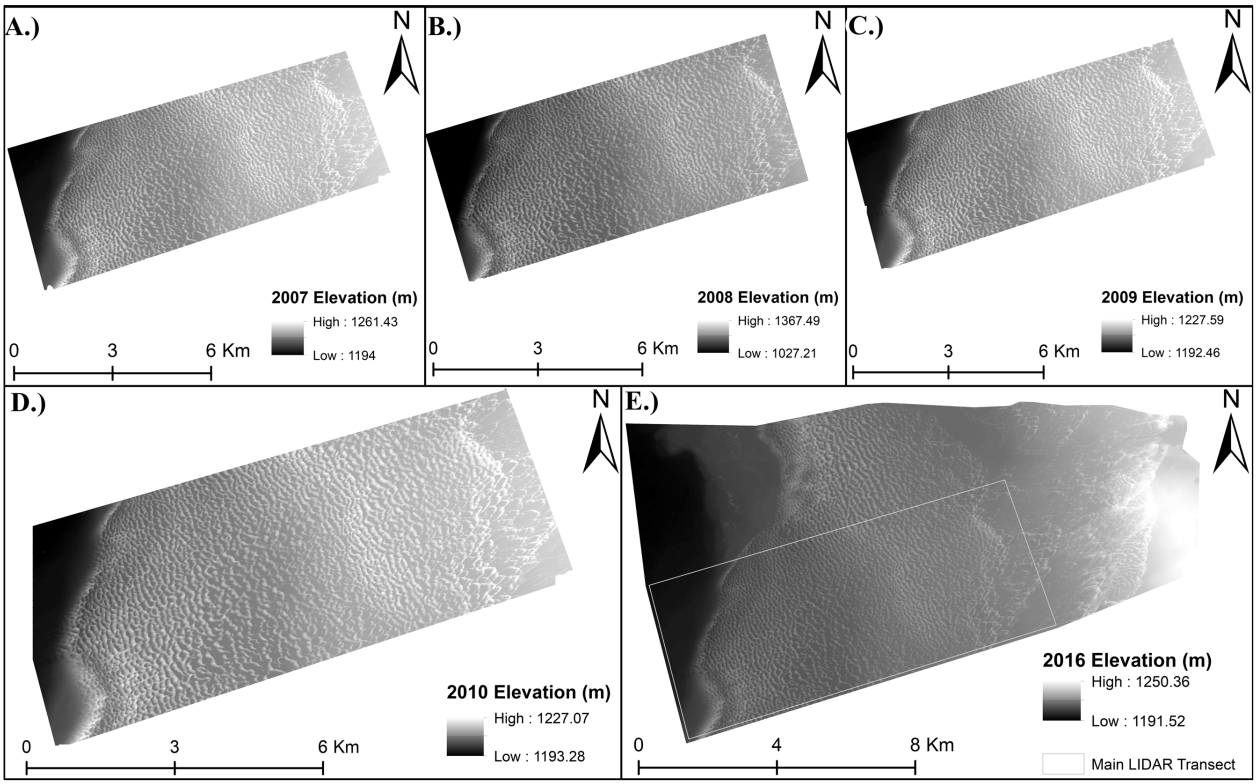

Figure 9. *A.)* Digital Elevation Model (DEM) of 2007 LIDAR survey detailing the heart of the dunes transect. *B.)* DEM of 2008 LIDAR survey detailing the heart of the dunes transect. *C.)* DEM of 2009 LIDAR survey detailing the heart of the dunes transect. *D.)* DEM of 2010 LIDAR survey detailing the heart of the dunes transect. *E.)* DEM of 2016 LIDAR survey detailing the heart of the dunes transect.

Additional remote sensing data was accessed through the Earth Explorer, a USGS data repository of satellite based remote sensing imagery. The types and key metadata are described in the methods when referencing their applications in the research.

CHAPTER 4

RESEARCH METHODOLOGY

4.1 Objectives

This study aims to accomplish three main tasks including (1) verifying the presence of IFLs within WSNP's dune field, (2) testing that the presence of lower salinity groundwater propagates stabilization, and (3) exhibiting the coupled control of groundwater salinity and aeolian processes upon dune mobility. The research plan will encompass a multifaceted approach using remote sensing techniques, field measurements, and geostatistical analysis.

4.2 Verify Presence of Inland Freshwater Lenses

4.2.1 Geospatial Analysis to Identify Field Sites

IFLs that form in arid regions have been shown to require conditions where they receive intense short rainfall events, have high infiltration rates, and reside on top of a highly saline unconfined aquifer (Milewski et al., 2014). In conjunction with the conditions specified above we determined a set of key variables to analyze that will be inputs into a modified approach of the technique used by Milewski (2014); groundwater salinity, vegetation type, soil moisture, and dune movement rate. The initial analysis was performed using geospatial image processing software (i.e., ArcGIS) to compile an integrated data platform used to delineate field sites for verification of lenses. Rate of movement, dune type, and digital elevation were derived from high resolution (1m x 1m x 0.4m) LIDAR data provided by WSNP. The LIDAR was preprocessed by Kocurek et al. (2012) and has records of being vertically proofed via control

points that were taken from 135 absolute ground points known to be non-moving structures (NPS picnic awnings, NPS restroom privy, pedestal dunes[2]) (Kocurek *et al.,* 2012). Difference maps were created from LIDAR of successive years (i.e., 2007-2008, 2008-2009, etc.) using the raster calculator tool in ArcGIS to subtract one year from the other. The LIDAR was used to assist in characterizing the three different dune formation zones that were identified and adapted from Langford's (2009) study (i.e., barchanoid, transitional, and parabolic) **(Figure 10)**.

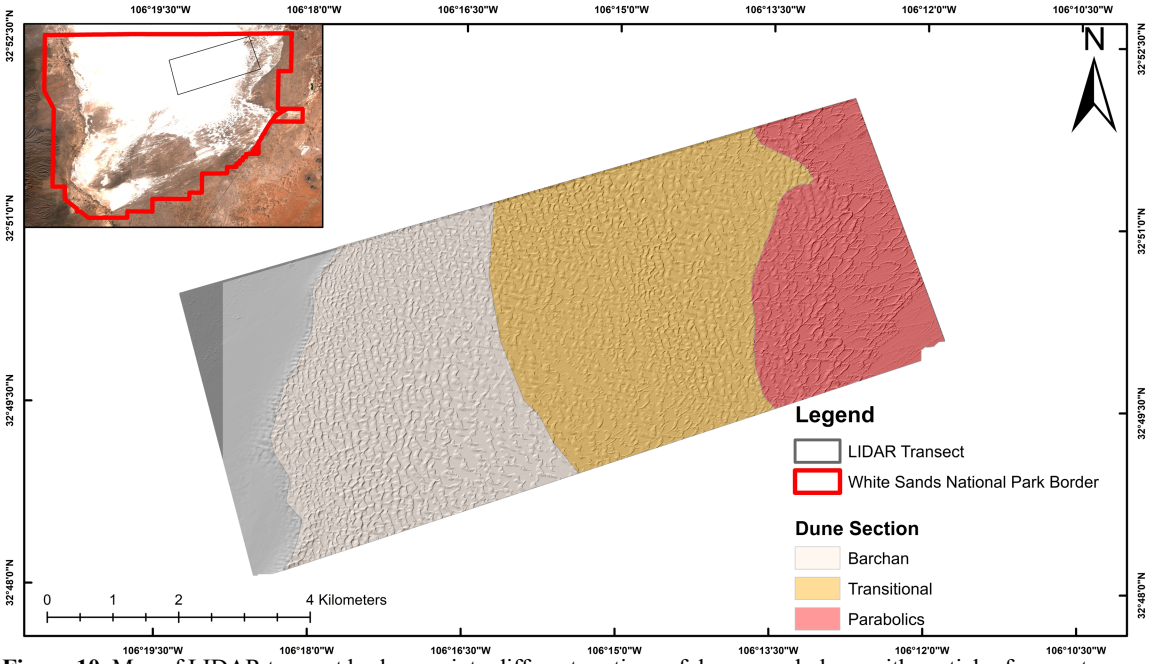

Figure 10. Map of LIDAR transect broken up into different sections of dune morphology with spatial reference to location in WSNP. Dune formation sections based on those seen in Langford *et al*. (2009).

The spatial difference maps were then used to take manual measurements of the leading edge of the slip faces on fifteen dunes in each dune field section via ArcGIS and used to calculate annual rates of migration **(Figure 11)**. Hydrologic characteristics (i.e., groundwater salinity and soil moisture) were taken from the existing well network, weather stations, and piezometers present in the park. Data from the WSNP well network was cleaned of NA values and over limit readings and used to make annual averages for groundwater salinity and soil

[2] Stabilized pedestal formed from vegetation transpiration and subsequent cementation of remnant dune held together by vegetation with a tap root system.

moisture across all recording depths from October 23rd, 2019 – October 23rd, 2020. The spatial difference maps, vegetation classification geodatabase (obtained from the NPS online portal and collected in 2016) and regional salinity and soil moisture interpolations were each designated an index to assign priority to desired characteristics **(Figure 12)**.

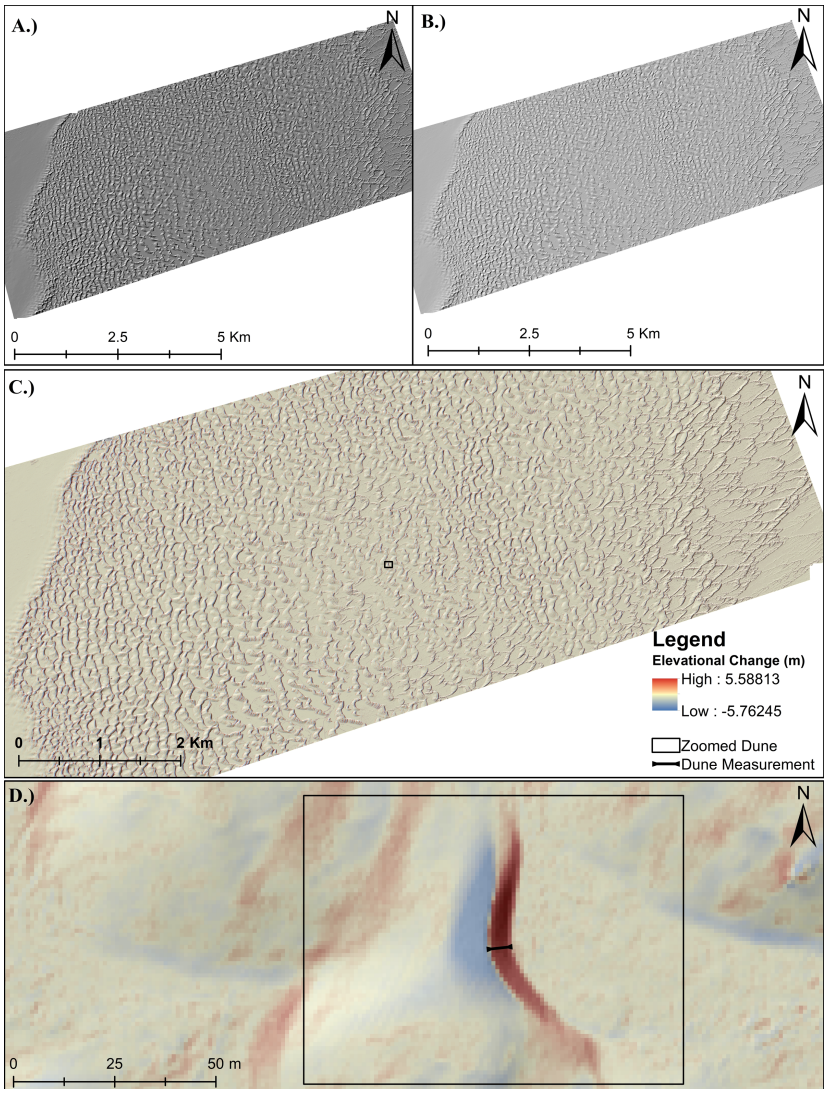

Figure 11. *A.)* January 2009 LIDAR transect with hill shade to highlight dune slip faces used in this spatial difference map. *B.)* June 2010 LIDAR transect with hill shade to highlight dune slip faces used in this spatial difference map. *C.)* Spatial difference map between 2009-2010 showing elevational changes in dune forms to highlight migration. *D.)* Zoomed in window of single dune showing where measurements are recorded from. Blue highlights 2009 slip face and red highlights 2010 slip face.

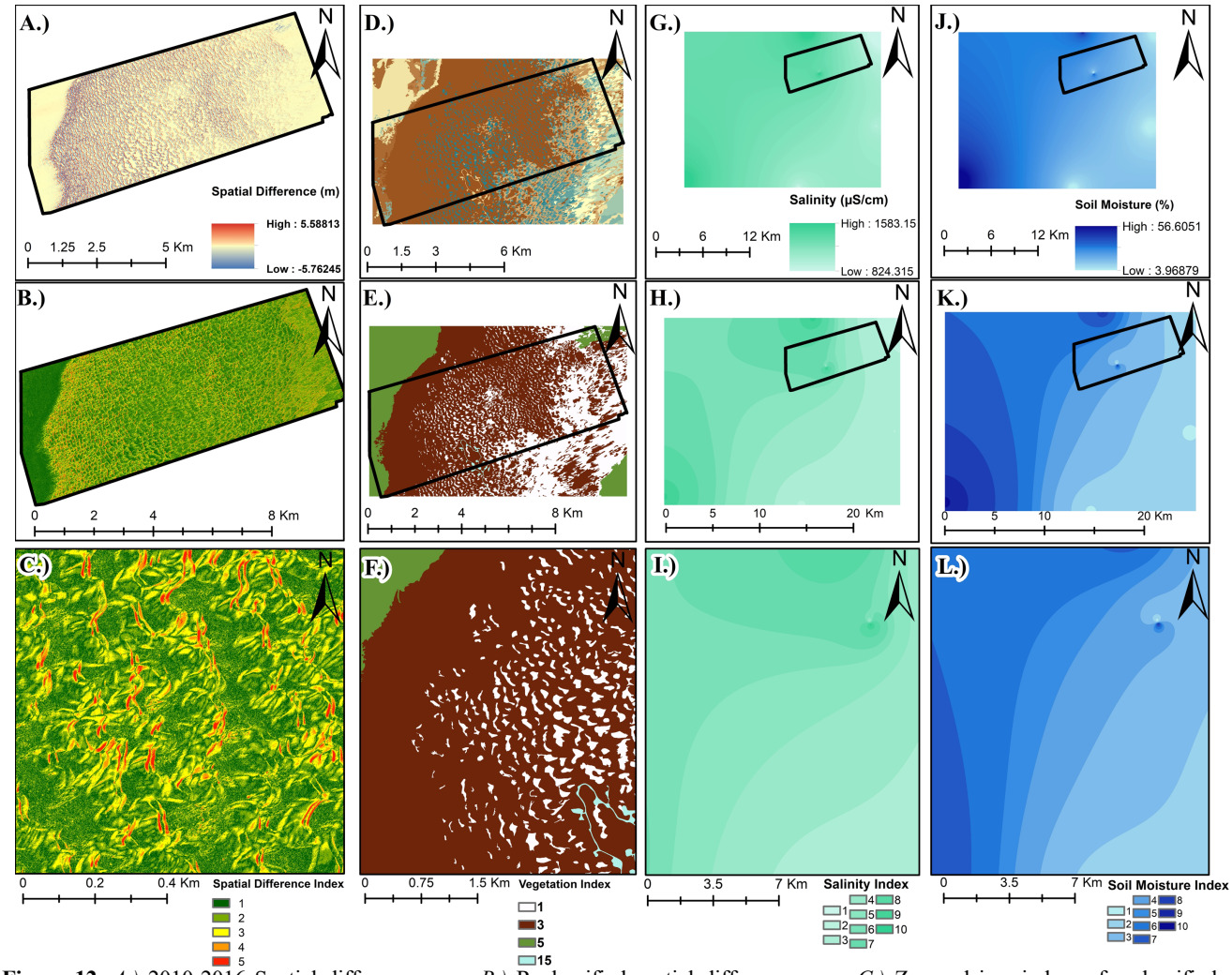

Figure 12. *A.)* 2010-2016 Spatial difference map. *B.)* Reclassified spatial difference map. *C.)* Zoomed in window of reclassified spatial difference map. Index set up so that values are classified via equal intervals in the data and any movement is assigned higher values (migration not of interest) and less movement is assigned lower values (interest in stability). *D.)* Clipped vegetation classification of study area collected by the NPS (2016). Legend included in *Data* section of *Study Site (Chap. 3)*. *E.)* Reclassified vegetation classification map. Index set so vegetated areas (1, highest interest), sparse vegetation/ barren dune (3), Alkali Flat (5), and roads (15, lowest interest). *F.)* Zoomed in window of reclassified vegetation map. *G.)* Interpolation (RBF) of groundwater salinity (all depths averaged) from WSNP well network data available (Oct. 2019 - Oct. 2020). *H.)* Reclassified map of groundwater salinity interpolation. *I.)* Zoomed in window of reclassified groundwater salinity map. Lower salinity is assigned lower values (of greater interest). *J.)* Interpolation (RBF) of soil moisture (all depths averaged) from WSNP well network data available (Oct. 2019 - Oct. 2020). *K.)* Reclassified map of soil moisture interpolation. *L.)* Zoomed in window of reclassified soil moisture map. Lower soil moisture is assigned lower values (of greater interest) due to space needed between surface and water table for an IFL to form.

The indexed data sets were assigned so that characteristics of interest would sum lower values on the overlay to indicate regions of interest for formation. The rankings are dimensionless and assign priority of potential to form an IFL in places with the lowest score. All variables were weighted equally due to the first order approach of this study and sparse literature on the existence of IFLs in this locale. The output is the preliminary Index Overlay (IO) map

(**Figure 13**) of places that are supposed to be ideal for IFL formation based on criteria of vegetation type, degree of spatial difference, soil moisture, and groundwater salinity (Milewski *et al.,* 2014; Kacimov and Obnosov, 2019). Given these characteristics, the interdune swales are highlighted due to the regular convergence of places where vegetation and minimal transport rate meet. Considering the calculated rates of migration, spatial trends in migration, and areas of interest (AOI) identified as ideal for IFL formation, locations within the park were then selected for well-installation and water sampling (**Figure 14**).

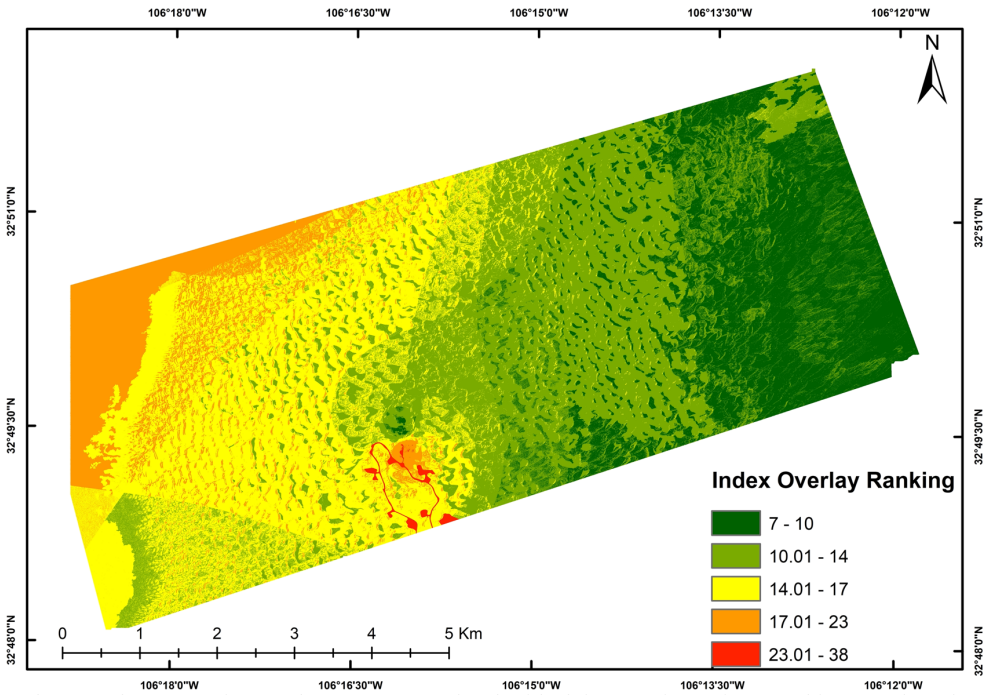

Figure 13. Index Overlay Map of areas that are supposed to be ideal for IFL formation. Rankings are based on sum of unitless assignments to characteristics of variables thought to be ideal for IFL formation. Lower values indicate more ideal for IFL formation. Interdune swales show as ideal formation sites throughout the transect due to the characteristics selected to characterize ideal formation, specifically minimal migration and denser vegetation.

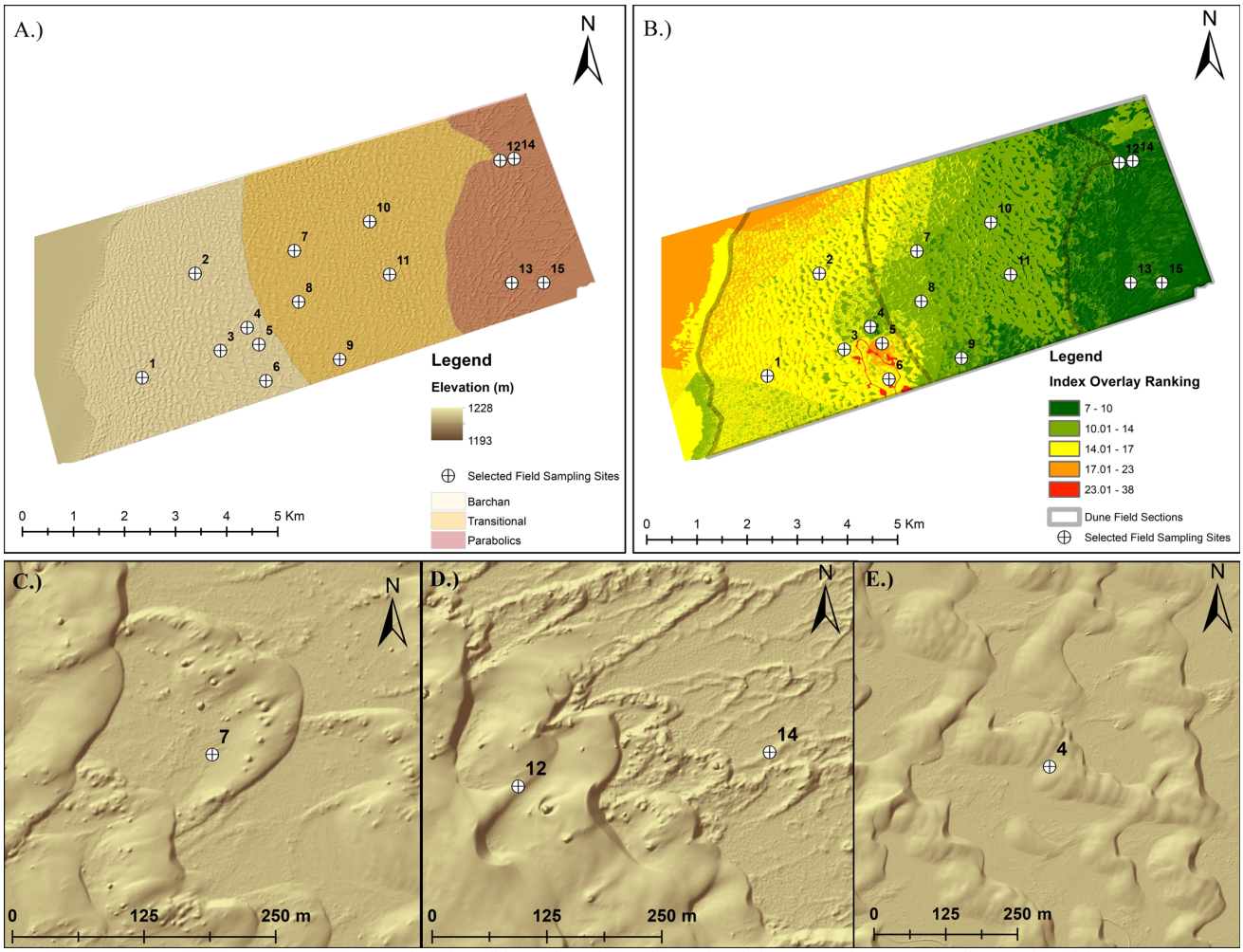

Figure 14. *A.)* June 2010 LIDAR survey showing fifteen locations determined for groundwater sampling. Mix of locations where IFLs are expected and locations where groundwater should follow regional trends *B.)* Index Overlay map for reference of where selected sampling sites are. *C.)* Close up of groundwater sampling site seven, partially selected due to dune morphology relative to regional trends of parabolic formation. *D.)* Close up of groundwater sampling site twelve and fourteen, partially selected due to abrupt transition into stabilized parabolic dunes. *E.)* Close up of groundwater sampling site four, partially selected due large interdunes.

4.2.2 Field Investigation

The field investigation was performed with the intention of identifying IFLs by assessing groundwater salinity. The field investigation was performed in the monsoon season (July-September) during August over three days from the 9th to the 11th. Groundwater was accessed through shallow (<2m) wells installed via hand-augered boreholes (**Figure 15)**. In situ measurement and water sampling took

Figure 15. Dr. Bob Craddock hand-augering a borehole for well installation in WSNP.

place in the three main dune formation settings (barchan, transition, and stabilized parabolic). At least 4 wells were installed in each dune formation setting based upon the initial visual inspection from the LIDAR and derived AOIs of expected IFL development. Wells were installed at locations 1-15, with the exception of Well 7B and 11.5 due to well casing supplies. All sites were sampled for in situ readings of conductivity, total dissolved solids (TDS), and salinity. An Oakton ExStik II EC400 conductivity probe was used to test water accessed through the wells as well as several additional locations of interest where wells were not installed. Groundwater samples were collected via bailers for further analysis to verify field readings of salinity due to gypsums propensity to dissolve in water and increase conductivity.

In situ measurements were used to refine preliminary interpolations of groundwater salinity from the preliminary geospatial analysis and detail the location of identified IFL formations. To validate measurements of key field locations, water chemistry was analyzed to identify the ionic species concentrations contributing to higher salinity. In particular, the concentrations of the following major cations and anions of interest, Ca^{2+}, Na^{+}, Cl^{-}, and SO_4^{2-}, were analyzed by Inductively Coupled Plasma Mass Spectrometry (ICP-MS). These ions were analyzed with the intent of identifying higher ionic concentration in areas with higher salinity/electrical conductivity and lower ionic concentrations in areas with lower salinity/electrical conductivity.

4.2.3 Post-Field Analyses

To corroborate field data collection and further identify patterns that coincide with IFL formation, additional remote sensing data sets were examined. The Normalized Difference

Vegetation Index (NDVI)[3] was applied to Sentinnel-2 imagery (10m) to detail conditions of vegetation health at a localized scale and Advanced Spaceborne Thermal Emission and Reflection Radiometer (ASTER) data were used to analyze soil moisture distribution using thermal bands[4].

ASTER thermal data (90m x 90m) were downloaded for dates closest to the time of in situ measurements and that encompassed as much of the study area as possible. Limitations were met with data availability that fit those specifications, thus one scene from August 23rd, 2021, was analyzed to estimate soil moisture conditions. The thermal product was downloaded, and Band 14 was extracted using ArcGIS. The Digital Numbers (DN) were converted to radians utilizing the *Raster Calculator* in ArcGIS by using **Equation 1** (Dar *et al.*, 2019):

$$CV_{R1} = (DN - 1) \times UCC$$

Where:

CV_{R1} is the cell value converted to radiance

DN is the digital number

UCC in the unit conversion constant

The UCC values were obtained from Abrams *et al.* (2001). The range from the NDVI was used to calculate Proportion of Vegetation (Pv) so that surface variable emissivity could be applied to the atmospheric correction and Land Surface Temperature (LST) calculations. Pv was calculated using **Equation 2** (Rouse *et al.*, 1974**)**:

$$Pv = \left(\frac{NDVI - NDVI_{min}}{NDVI_{max} - NDVI_{min}}\right)^2$$

[3] Remote Sensing technique using ratio of Near Infrared (NIR) and red spectral bands to identify vegetation health. Equation: NDVI=(NIR-Red)/(NIR+Red)

[4] Thermal bands are electromagnetic waves captured via sensors that are in the range of 8-14 μm.

The product was used to calculate surface variable emissivity using the **Equation 3** (Sobrino *et al.*, 2008):

$$\varepsilon_v = .85 + (.07 \times Pv)$$

Where:

ε_v surface variable emissivity

.85 is the emissivity of gypsum (Engineering Toolbox, 2003)

.07 is the difference between gypsum emissivity and sparse vegetation emissivity (Engineering Toolbox, 2003)

The emissivity product was input into the atmospheric corrections using the following **Equation 4** (Coll *et al.*, 2005; Dar *et al.*, 2019):

$$CV_{R2} = \frac{CV_{R1}}{\varepsilon_v \tau} L\uparrow - \frac{1 - \varepsilon L\downarrow}{\varepsilon_v}$$

Where:

CV_{R2} is the atmospherically corrected radiance cell value

τ in the transmittance

$L\uparrow$ is the Upwelling radiance

$L\downarrow$ is the Downwelling radiance

The upwelling radiance, downwelling radiance, and transmittance were obtained from the NASA Atmospheric Correction Parameter Calculator. With the image in atmospherically corrected radiance the conversion to Land Surface Temperature (LST) was made. The LST product is in Kelvins. The relationship between LST and NDVI was used to calculate the the Soil Moisture Index (SMI). The LST product was calculated using **Equation 5** (Dar *et al.*, 2019):

$$LST = \frac{K_2}{(\ln(\frac{K_1}{CV_{R2}} + 1) \times \varepsilon_v}$$

Where:

K_1 and K_2 are pre calibrated constant values (Abrams and Hook, 2001)

The LST and NDVI were then used to calculate the SMI via **Equation 6 (**Parida *et al.*, 2013; Saha *et al.*, 2018)

$$SMI = \frac{LST_{max} - LST}{LST_{max} - LST_{min}}$$

Where:

LST_{max} = m NDVI + b from the warm edge of the data

LST_{min} = m NDVI + b from the cold edge of the data

The product of the SMI, NDVI, and in situ readings were used to make inferences about spatial trends and to extract data for latter objectives.

4.3 Test that the Presence of Lower Salinity Groundwater Propagates Stabilization

To assess the relationship between vegetation and dune stabilization the NDVI was applied to Sentinnel-2 satellite imagery at 10m x 10m resolution from Aug 6th, 2021 to identify vegetation stress in locations that were sampled for ground water. Values derived from this analysis were then compared against groundwater salinity measurements from the field using a linear regression. A secondary linear regression was applied looking at the relationship between dune mobility (derived from the 2010-2016 LIDAR difference map) and vegetation health at the same sites. Another Sentinnel-2 satellite image at 10m x 10m resolution from Aug 6th, 2016 was used to extract vegetation health values to compare against the most recent LIDAR surveys. The variables were compared against vegetation due to the nature of the recognized significance of vegetation impact upon dune field transitions (Bagnold, 1941; Lockwood, 1995; Durán and Herrmann, 2006; Reitz et al., 2010; Jerolmack et al., 2012).

4.4 Exhibit the Coupled Control of Groundwater Salinity and Aeolian Processes Upon Dune Stability

A study performed by Langford (2009) laid the groundwork for examining the concept of groundwater salinity influencing the stabilization of dunes, however more in-depth measurements are needed to expand upon his preliminary findings. Thus, in order to exhibit the multidimensionality of controls upon this system we utilize a 3-D Cluster analysis. The analysis was performed using data from the prior components of the study to define the axes by the speed of movement of the dune (Y-axis), distance from the Central Dune Ridge (CDR) (X-axis), and salinity of the groundwater (Z-axis). Data integration was done through coding in R to coalesce the different data sets and produce the three-dimensional graph for analysis. K-Means clustering method[5] was applied to the data to group field sites to see if they clustered based a particular controlling factor.

[5] Statistical method for clustering points based on the sum of squares of the distances from the mean vector. Number of clusters are predefined, and all points are compared to means within the set and grouped with the average they are closest to.

CHAPTER 5

RESULTS

5.1 Verifying Presence of Inland Freshwater Lenses

5.1.1 Geospatial Analysis to Identify Field Sites

Upon visual inspection of the difference maps it is evident there is a large section of the dune field toward the center of the barchan and transitional sections where dune movement slows **(Figure 16)**. Measured dune movement shows variation based on the section of the dune field with barchan moving the fastest at an average rate of 7.65 m/yr from 2007-2010. From 2007 - 2010 the LIDAR surveys show the average rates of dune movement consistently descending across the active barchanoid dunes toward the more stabilized parabolic dunes. The rate of movement (m/yr) for 08-09 show an average of 43.6% increase in movement from 07-08. From comparing 2009-2010 to 2007-2008 there is a 25.5% decrease in movement. Dune movement in the parabolic region shows up to 70.48% increase in migration rate in response to the stabilizing controls (i.e., vegetation, increased soil moisture, decreases groundwater salinity, and decreased aeolian influence). In conjunction with the measurements in **Table 1** the dunes measured for pre-field analysis can be seen in **Figure 16.**

Table 1. Annul average dune rates calculated from ArcGIS manual measurements of spatial difference maps from sequential LIDAR transects between 2007-2010. Annual rates accounted for by considering dates between collections.

	Barchan	**Transitional**	**Parabolic**
07-08 Dune Rate (m/yr)	7.27	5.22	1.78
08-09 Dune Rate (m/yr)	10.11	7.26	3.15
09-10 Dune Rate (m/yr)	5.55	3.26	1.82
07-10 Dune Rate (m/yr)	7.65	5.25	2.25

The interpolations made from the well network data **(Figure 17)** show regional trends of decreasing salinity moving from the eastern margin of the dune field to the west, with increasing salinity toward the northern border near the beginning of the alkali flats in an area heavily vegetated that does not contain dunes. The interpolation of the soil moisture gradient follows a similar trend to groundwater salinity, increasing in the north near the start of the Alkali flat and increasing moving east to west.

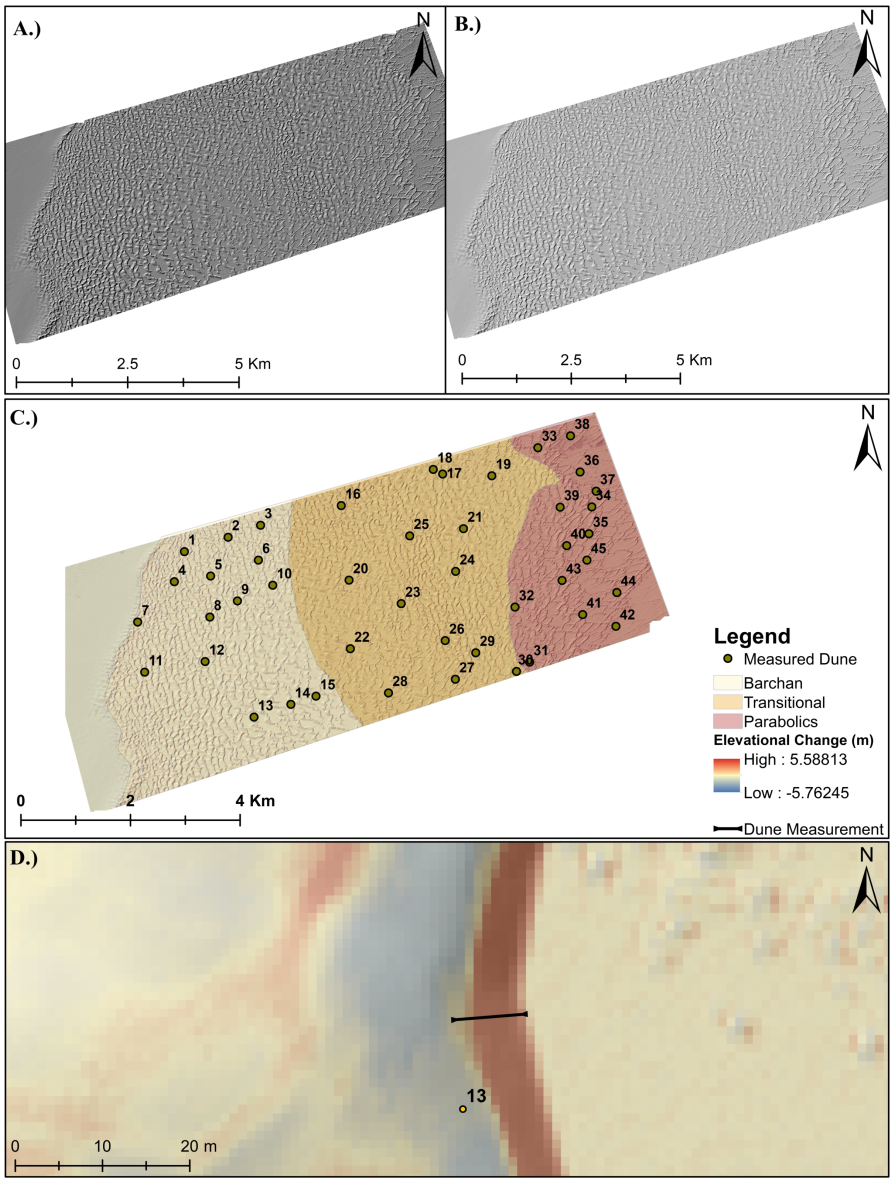

Figure 16. *A.)* January 2009 LIDAR transect with hill shade to highlight dune slip faces used in this spatial difference map. *B.)* June 2010 LIDAR transect with hill shade to highlight dune slip faces used in this spatial difference map. C.) Spatial difference

map between 2009-2010 showing elevational changes in dune forms to highlight migration and divided into dune formation zones. *D.)* Zoomed in window of Dune 13 showing where measurements are recorded from. Blue highlights 2009 slip face and red highlights 2010 slip face.

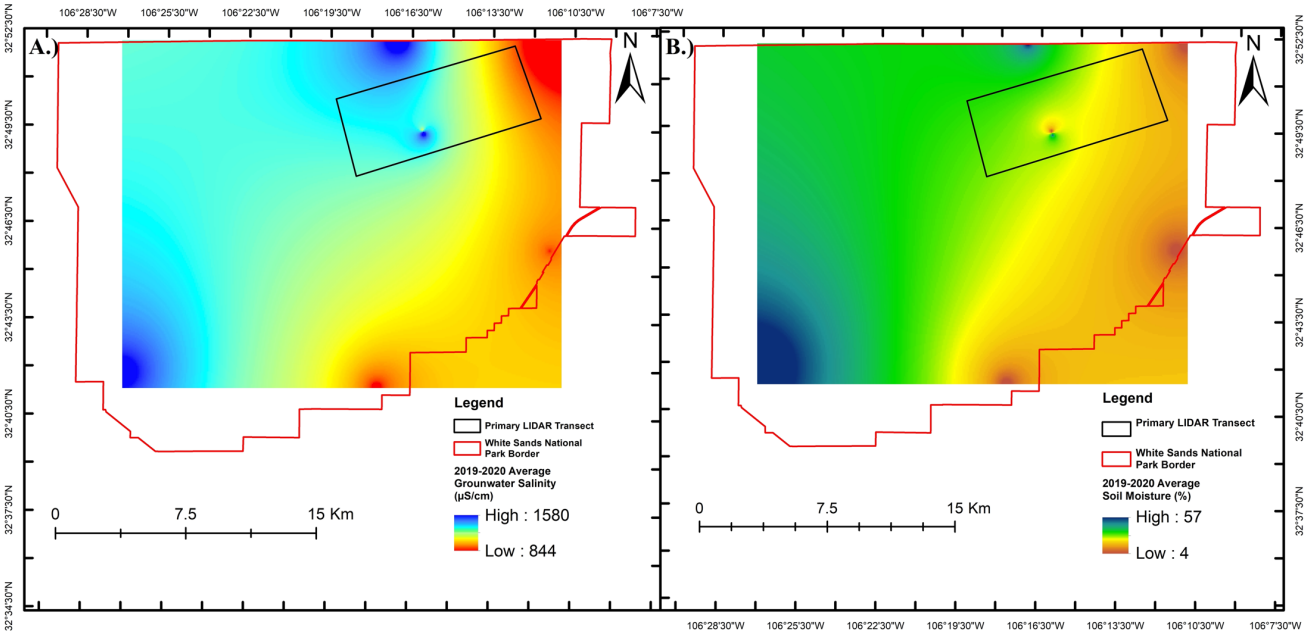

Figure 17. *A.)* Radial Basis Function interpolation of average annual groundwater salinity from WSNP well network. *B.)* Radial Basis Function interpolation of average annual soil moisture content from WSNP well network.

The results of the index overlay map (**Figure 13**) prioritized the eastern half of the dune field to be ideal for the formation of IFLs and additionally highlighted the interdunes in the more mobile part of the dune field as a good formation setting. The results of the analysis seen in **Figure 13**, as well as visual inspection of patterns in dune field morphology from the LIDAR surveys, led to determining the groundwater sampling locations seen in **Figure 14**.

5.1.2 Field Investigation

Groundwater sampling took place at the locations specified in **Figure 18.** The readings can be seen below in **Table 2** with coordinates and one additional site not pictured in primary map on Figure 15, due to it not being where any of the LIDAR surveys were performed.

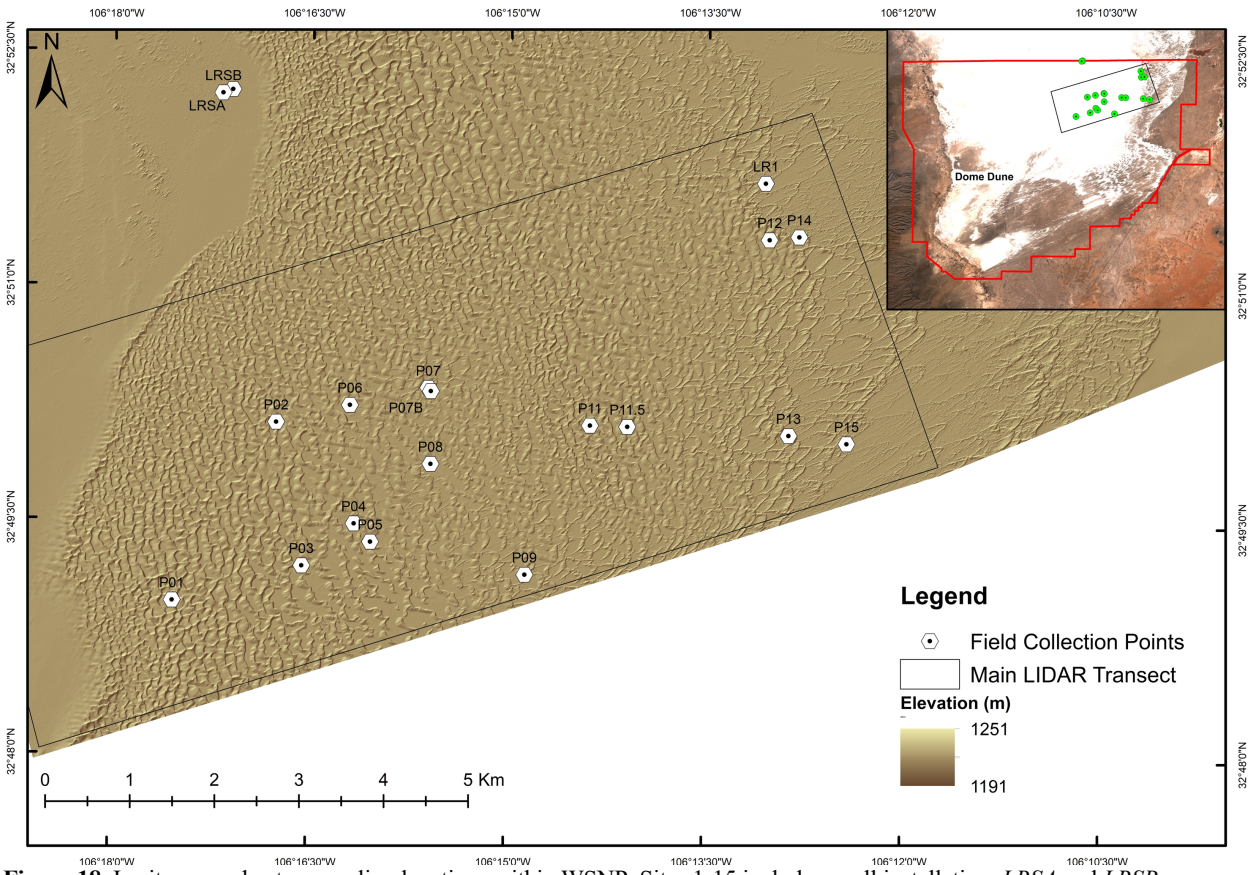

Figure 18. In situ groundwater sampling locations within WSNP. Sites 1-15 include a well installation. *LRSA* and *LRSB* are surficial springs. *LR1* is where the Lost River dissipates into the groundwater table. The distant site seen in the spatial reference window shows where the last believed dome dunes exist in the park and that site was sampled for water but not included in the primary map since it is not within the extent of any of the LIDAR surveys obtained.

Table 2. In situ sampling of basic physical properties of water at sites within WSNP. *OL* stands for Over Limit. "-" signifies reading was not recorded. Depth to water from the surface is abbreviated as *DTW.* The DTW and elevation were used to calculate the water table elevations (WT elevation).

ID	Northing	Easting	Elevation (m)	DTW (m)	Total Depth (m)	Conductivity (mS/cm)	Temperature (°C)	Salinity (‰)	TDS (‰)	WT Elevation (m)
LR1	386068	3636582	1212.13	-	-	OL	-	OL	OL	-
LRSA	379772	3637703	1202.07	0	0	6.11	29.5	3.36	4.29	1202.07
LRSB	379656	3637663	1204.21	0	0	5.28	28.2	2.88	3.7	1204.21
P01	379043	3631669	1206.03	0.61	0.82	2.46	27.8	1.73	-	1205.42
P01B	379028	3631666	1205.43	0.43	0.70	2.81	28.2	1.95	-	1205.00
P01C	379014	3631668	1201.77	1.04	1.40	2.94	28.7	1.54	-	1200.73
P02	380278	3633771	1205.43	0.50	0.98	5.5	26.5	3.85	-	1204.93
P03	380575	3632072	1203.60	0.55	0.96	19.2	25.1	11.38	13.5	1203.05
P04	381194	3632568	1206.64	2.23	2.47	4.46	23.3	3.08	-	1204.41
P05	381388	3632352	1208.47	0.47	0.72	9.22	25.6	5.15	6.48	1208.00
P06	381151	3633970	1206.95	0.85	1.43	4.06	27.2	2.18	2.81	1206.10
P07	382077	3634170	1208.78	0.60	0.89	3.79	26.4	2	2.65	1208.18
P07B	382107	3634132	1209.08	0.59	0.94	4.67	25.5	2.52	2.24	1208.49
P08	382102	3633271	1207.25	2.16	2.69	4.88	23.7	2.67	3.43	1205.09
P09	383212	3631961	1209.39	0.76	1.34	3.67	25.7	1.96	2.56	1208.63
P11	383988	3633723	1211.22	0.42	1.01	2.58	23.2	1.34	1.81	1210.80
P11.5	384429	3633709	1215.79	0.59	1.18	2.88	23	1.5	2.01	1215.20
P12	386114	3635914	1214.87	0.60	1.09	2.8	25.4	1.46	1.95	1214.27
P13	386335	3633600	1215.48	2.07	3.10	3.55	22.6	1.88	2.48	1213.41
P14	386465	3635948	1216.09	0.92	1.44	3.35	25.4	1.77	2.35	1215.17
P15	387020	3633503	1213.96	1.39	1.92	5.85	24.3	3.21	4.11	1212.57
Dome	371161	3624675	1192.01	4.79	5.70	OL	20.3	OL	OL	1187.22

The above data was used to create the interpolation of the groundwater salinity gradient (**Figure 19)**. No OL readings could be incorporated (LR1 and Dome). There is a dramatic increase in salinity in the area near the roads and steep decline in the far southwest corner of the interpolation. The regional gradient trends as expected with lower salinity in the east and higher in the west toward the Alkali Flat. All groundwater sampled within the dune field was less than 2.5 m in depth below the surface. The water table elevation was lowest in the west and highest in the east.

The results from the ICP-MS analysis are displayed in **Table 3**. The samples that presented the higher reading of EC/salinity in the field also present higher ionic content. A direct comparison of the water chemistry, in terms of concentrations of ionic species, and EC isn't possible in our case, because of ions that were not analyzed (HCO_3^-, Mg^{2+}, K^+) due to limited funding. Additionally, potential dissolution of gypsum sediments in the water samples occurred in between sampling and analysis, as reflected by the very high concentrations in sulfate.

Table 3. ICP-MS readings of six key groundwater samples collected within WSNP.

Well Number #	^{23}Na ppm	^{43}Ca ppm	Chloride ppm	Sulfate ppm
P01	34.03	270	36.55	1,971.78
P03	996.7	205.7	2,055.28	3,452.44
P04	262.6	191.9	521.15	2,094.22
P07	175.6	205.8	381.75	2,313.58
P11	30.15	188.2	47.49	1,554.63
P12	44.18	212.1	71.57	1,530.47

The interpolation of in situ groundwater salinity readings show a higher resolution of the groundwater salinity gradient throughout the sampled area of the dune field. A Radial Basis Function in ArcGIS was applied to the data and can be seen in **Figure 19** below. The radial basis function was chosen due to its ability to recognize values beyond the maximum/minimum and create smooth transitions, exemplary of a regional salinity gradient change. It is not ideal for

characterizing the extent of the IFL in the barchan section due to the sharp change in groundwater salinity over short distances, however it works well for the gradual transition seen throughout the dune field.

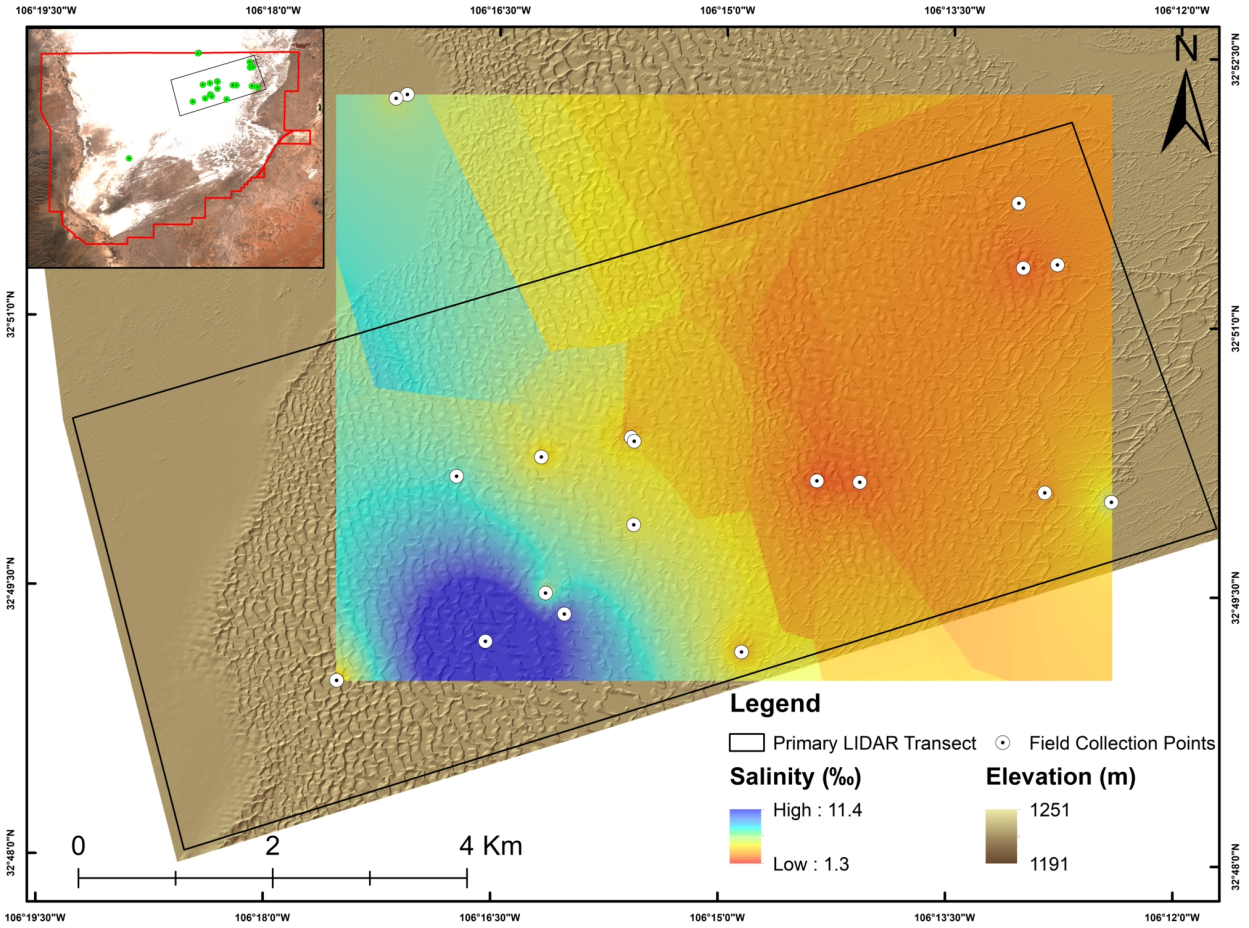

Figure 19. Radial Basis Function interpolation of groundwater salinity (‰) gradient as determined from in situ measurements collected during the field investigation in WSNP. Gradient follows general trend of that determined from WSNP well network but also highlight the discovery of an IFL in the barchan section of the dune field.

5.1.3 Post-Field Analysis

Vegetation health shows a trend that closely mirrors the groundwater salinity gradient determined via in situ groundwater sampling, where vegetation health is higher in the east and lower in the west. Localized anomalies to the general trend appear within the barchan area on the scale of 1-5 pixels, identifying Salt Cedar trees (**Figure 20**) as well as larger swaths of higher

vegetation health toward the middle of the transect. The SMI in **Figure 21** shows higher values in the east and similarly matches up with areas of higher soil moisture toward the center of the transect. The areas with both high soil moisture and healthier vegetation also both contain lower groundwater salinity with the exception of the IFL located in the barchan on the far western side of the in situ sampling locations utilized to make the interpolation.

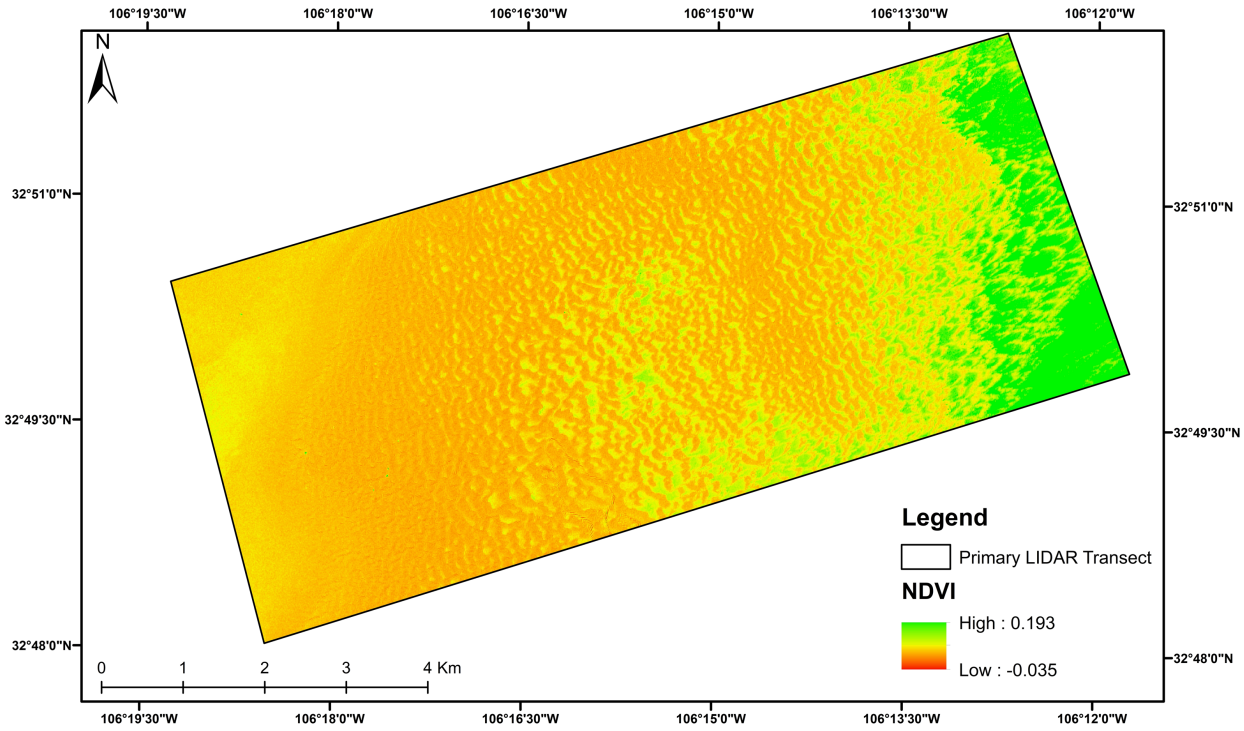

Figure 20. Map of NDVI applied to Sentinnel-2 imagery (10m x 10m) from Aug 6th, 2021 of WSNP heart of dune transect area to highlight variability in vegetation health throughout transect. Green areas highlight vegetation reflecting more NIR/Red light, signaling less stressed vegetation. All areas with evidence of parabolic dune structure have a greater amount of healthy vegetation. NDVI values classifying healthy vegetation are low compared to typical standards but represent the sparse vegetation cover and harsh conditions throughout even the areas that relatively densely vegetated for this setting.

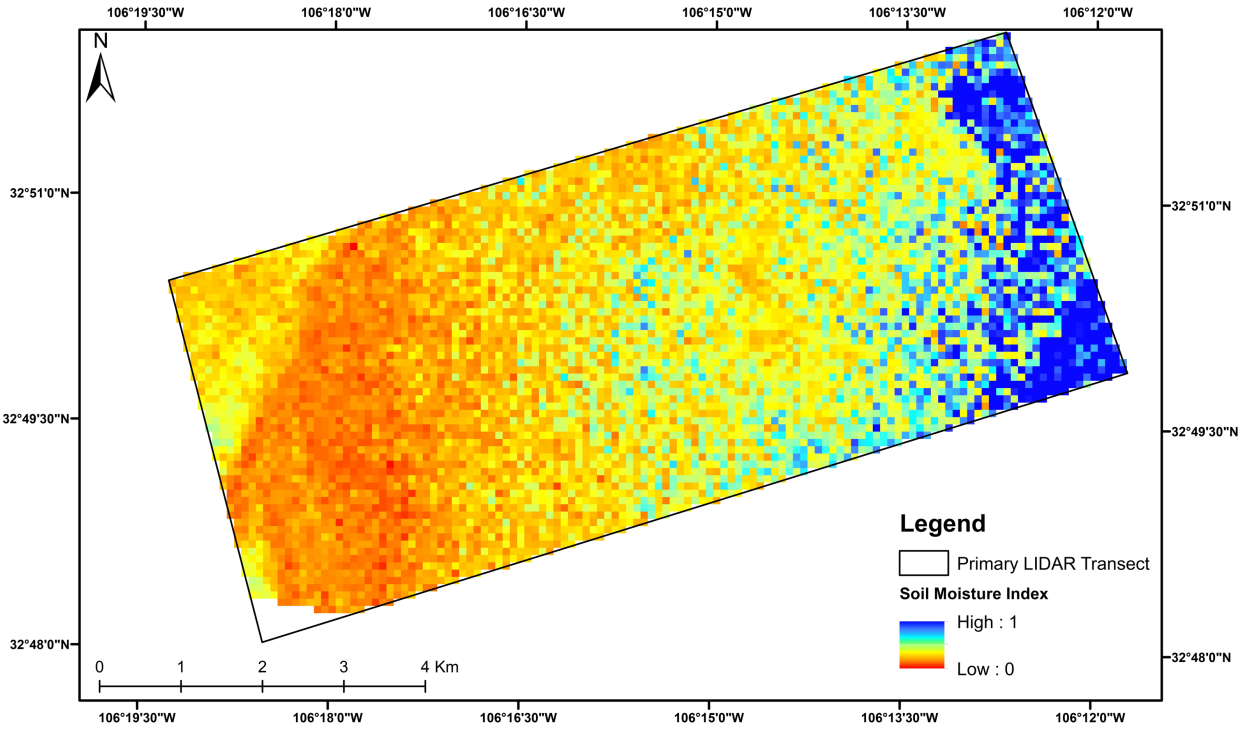

Figure 21. Soil Moisture Index applied to ASTER imagery (90m x 90m), collected on Aug 23rd, 2021, heart of dune transect area. The SMI accounts for the relationship of LST and NDVI to classify where soil moisture is high comparatively within the area of interest. The soil moisture trend closely follows healthy vegetation cover as well the salinity gradient, but also the trends to higher soil moisture in areas where dune movement slows.

5.2 Test that the Presence of Lower Salinity Groundwater Propagates Stabilization

The linear regression of dune migration rate modeled as a function of vegetation health resulted in an adjusted R^2 of 0.466. The intercept (4.3323) has a p-value of $1.29 \cdot 10^{-5}$ and the slope (-42.7523) has a p-value of 0.00214. The plot of this linear regression model can be seen in **Figure 22**. The linear regression of vegetation health modeled as a function of groundwater salinity resulted in an adjusted R^2 of 0.01471. The intercept (0.043688) has a p-value of 0.00556 and the slope (-0.003874) has a p-value of 0.28724. The plot of this linear regression model can be seen in **Figure 22**.

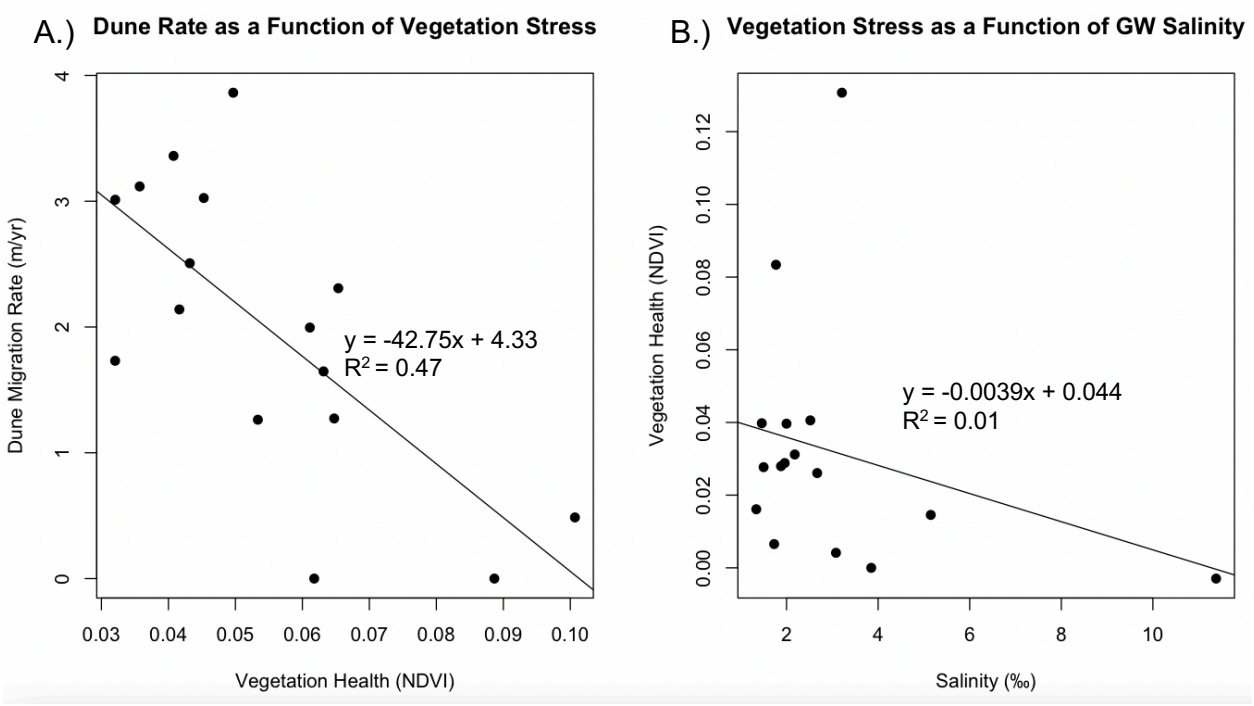

Figure 22. *A.)* Linear regression of dune migration rates as a function of vegetation health. Vegetation health was calculated through band math by applying the NDVI to Sentinel-2 data collected November 30th, 2016. Dune migration rates were calculated from measurements taken on spatial difference maps utilizing the June 2010 and Jan. 2016 LIDAR surveys. *B.)* Linear regression of vegetation health as a function of groundwater salinity. Vegetation health was calculated through band math by applying the NDVI to Sentinel-2 data collected Aug. 6th, 2021. In situ groundwater salinity measurements were taken between Aug. 9th – 11th, 2021.

5.3 Exhibit the Coupled Control of Groundwater Salinity and Aeolian Processes Upon Dune Stability

Cluster One is made up of a single point with high groundwater salinity and barchan morphology. All points prior to the 4 km mark are barchan and groundwater salinity varies from highly saline to fresh. Cluster Two is composed of all other values before 5 Km. It is a mix of both parabolic and barchan dunes. Salinity values in this cluster are saline to fresh. All points after 5 Km make up Cluster 3 and contain mainly fresh water, with exception of one point being brackish. All points in this cluster are parabolic dunes except for one that is barchan. The plotted cluster analysis can be seen below in **Figure 23**. The Between Sum of Squares (BSS) to Total Sum of Squares (TSS) is 79.5%.

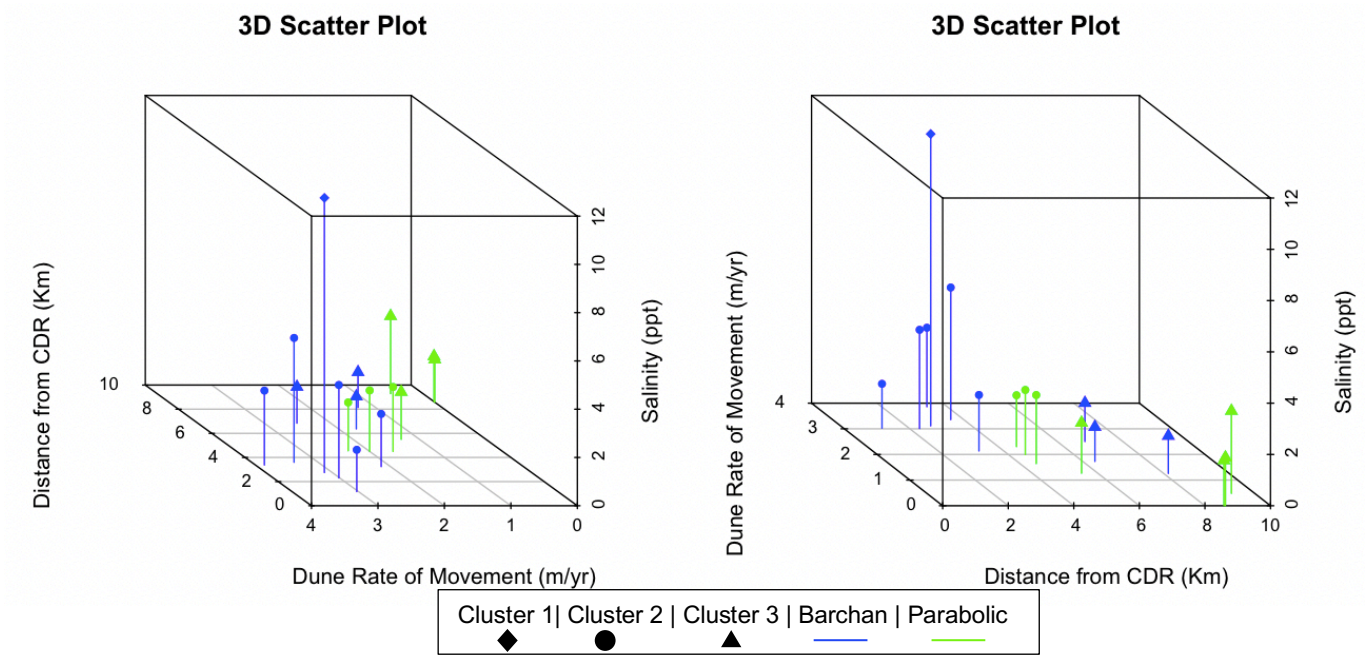

Figure 23. 3-Dimensional Cluster Analysis of sites within WSNP. Dune rate calculated from 2010-2016 difference map of LIDAR surveys. Distance from CDR measured in ArcMap from LIDAR surveys. Distance from the CDR is a proxy for degree of aeolian influence. Groundwater salinity is from in situ measurements via hand augered boreholes. Points are grouped in to 3 clusters via K-means (shape) and colored based on dune morphology. The two figures are the same the same values plotted from different perspectives to fully be able to visualize the data.

CHAPTER 6

DISCUSSION

This chapter will follow the structure seen in the previous chapters, addressing each objective and their implications. Suggestions for future work and improvements to the techniques implemented are detailed with in each section as well. In this chapter an additional section discusses a conceptual model that explains the current understanding of the regional groundwater salinity gradient in relation to the dune form transitions.

6.1 Verifying Presence of Inland Freshwater Lenses

6.1.1 Geospatial Analysis to Identify Field Sites

The use of LIDAR to track dune field patterns allowed for very precise tracking of dune migration patterns on a spatial scale. The incorporation of consistent surveying on a monthly or seasonal scale would allow for more insight as to the seasonal variation in dune migration rates and subsequently what other characteristics vary accordingly to distinguish controls upon dune migration.

The results of the IO map successfully identified field sites that would propagate the formation of IFLs as can be seen from the in-situ readings collected and further verification of ICP-MS analysis. Although the method worked, its predictive power could be increased through the incorporation of higher resolution data on both a temporal and spatial scale. Weighting the variables equally would have allowed for a better understanding of the controlling factors of IFL development and prevented the over prioritization of any variable given the lack of knowledge on the existence and formation of IFLs in this location. The indexes applied were arbitrary,

however they allowed for a simplified view of understanding where the desired characteristics overlapped. In the future a Geographically Weighted Regression model could increase the capability to recognize locations that should be ideal for IFL formation; however, given the data limitations of this study that approach was not used.

One of the main limitations was the sparse geochemical data. There were only 7 wells to interpolate the groundwater characteristics, and they that were not equally distributed. Well data quality was also in question. Units of groundwater salinity were assumed to be in µS/cm; however, the units were listed in an unknown unit (VIC) that was unidentifiable through research nor park staff. These readings would also insinuate a relatively fresh groundwater table throughout the entire dune field, which is inconsistent with the findings of any previous studies. Regardless of units, it did allow for interpretation of a rough gradient for both soil moisture and groundwater salinity that was consistent with the change in the gradient discovered through the in situ measurements.

6.1.2 Field Investigation

In situ measurements of groundwater salinity support the existence of a localized (m^2) IFL in the barchan section of the dune field that is dominated by saline groundwater. Measurements for groundwater salinity at well P01 were of the freshest recorded values in the field with all three readings taken at that location (P01, P01-B, P01-C) showing values below 2.00 (‰). Additionally, this is supported by the conceptual model created by Kacimov and Obnosov (2019) in which the lens can exist in the topographic mound created by the dune. The relatively consistent temperature throughout the majority of the dunes internal structure (excluding the shallow surface within roughly the first foot of sediment) prevents evaporation and allows recharge to infiltrate and remain within the dune. The density differences between

the saline and fresh groundwater prevent mixing and the pressure potential within the dune sediment likely adds to this effect and creates conditions ideal for the sustained formation of IFLs in the dunes of the barchan section of the WSNP dune field. More diagnostic measurements are needed quantify this relationship and understand the mechanisms that propagate IFLs in only some of these dunes while not in others.

With little precipitation in the days prior to the sampling the likelihood of dilution skewing measurements seems implausible given the regional groundwater salinity gradient. The regionally fresher groundwater to the east needs further investigation before any conclusive interpretations can be made about its source. We considered a source for the fresh groundwater given previous literature (Bourret, 2015) modeling the upwelling of remnant and regional groundwater around the Jarilla fault, however issues for this concept arise from the concentration of dissolved salts that compose the chemical profile of these waters due to their extended travel times through highly carbonate and evaporite rich layers. These waters make up a large proportion of the input of groundwater in the dune field but do not explain fresh groundwater presence. Given the topographic rise toward the east a regional (km^2) IFL is likely a good explanation, however more work needs to be done to characterize the saline to fresh groundwater interface and confirm this hypothesis.

The ICP-MS analysis matches closely with the in-situ groundwater salinity readings, although there are slight differences that are likely accounted for by the analysis of only several components of the chemical profile due to limited funding on the project. The changes in the trends of the NDVI, SMI, and groundwater salinity all match closely with areas where dune migration patterns shift from mobile to less mobile. Specifically, where salinity lowers, soil moisture rises, and vegetation is healthier, dunes are less mobile. Due to limited time in the field

only a select number of sites could be sampled and the identification of additional IFLs in the barchan section of the dune field would give better insight about the formation setting needed. To aid in further understanding IFLs forming in the area, longer term tracking of groundwater chemistry at confirmed sites and geophysical characterization of the confirmed IFL sites would show the temporal scale upon which these formations change seasonally. Additionally, determining the geometry of the IFL will be valuable in characterizing their formation setting more definitively. The IFL extent in the barchan section of the dune field shown in the interpolation of the field readings does not accurately represent the change from fresh to saline groundwater. This is due to the sharp change in salinity concentration and the limitations of the Radial Basis Function to accurately predict large changes in short distances.

6.1.3 Post-Field Analysis

The spatial trend analysis gives valuable insight to the fact that there is a relationship between groundwater salinity, vegetation, and soil moisture upon the stabilization of the dunes and highlights that there is a missing component to understanding dune mobility. One may postulate this is the availability of the fresher water to vegetation, and that as the topography changes on both a very localized scale (mounding of the dune and the inter dune swales) and regional scale (rise from Alkali flat toward the east and paleo shorelines of Lake Otero) the surface to groundwater table difference changes and can limit vegetations ability to reach fresh groundwater.

Additionally, the calculation of the LST skews the accuracy of the SMI due to sensor limitations to penetrate the surface. Thus, accurately assessing the soil moisture is complicated by the fact that the temperature values entered are only estimating soil moisture for the

shallowest depths of the surface. Due to the dune's cooler internal temperature, soil moisture has the potential to increase drastically with depth and less losses to evaporation.

6.2 Test that the Presence of Lower Salinity Groundwater Propagates Stabilization

The control upon dune migration from vegetation shows a weak relationship (adjusted R^2= 0.466). However, given the statistical significance of the slope (p = 0.002139) we can reject the null hypothesis that dune migration is not impacted by vegetation health. Increasing the resolution of the imagery used to calculate the NDVI could better describe the density of healthy vegetation, which is relatively hard to identify given the sparse distribution of vegetation in many of the interdunes and the spatial resolution of the imagery being limited to 10m x 10m. Some species, for instance *T. Gallica*, have high impact upon stabilizing sediment (creating pedestal dunes) but do not grow closely with other vegetation and thus may not be identified from a single pixel. Another likely component of unexplained variance is the degree of stability applied from different plant species. Further classification of the plant species in conjunction with the vegetation stress could help to eliminate a large portion of unexplained variability.

The results of the linear regression between vegetation stress and groundwater salinity show no direct relationship (adjusted R^2= 0.01471) with no significance to the slope (p= 0.28724). This is likely not diagnostic of the relationship. The data here does not classify the vegetation by species which has a large impact upon the degree of stress induced upon different plants species as well as the previously mentioned issues surrounding the spatial resolution of the NDVI applied. *T. Gallica*, when large enough to be recognized via the resolution at which data was collected, can effectively succeed in highly saline conditions where little vegetation of other species is shown to survive. The collection of additional groundwater readings in conjunction

with a detailed vegetation classification could better describe the relationship and give insight as to how much groundwater salinity in this region effects vegetations ability to grow.

6.3 Exhibit the Coupled Control of Groundwater Salinity and Aeolian Processes Upon Dune Stability

K-means clustering successfully partitioned the data in to three groups. Cluster one seems to be characterized by the extremely high salinity relative to the other groups. This group could be classified as aeolian dominated based on the location relative to the CDR, fast rate, and lack of fresh groundwater or healthy vegetation. Cluster Two is characterized by multiple dune types and varying groundwater salinity from fresh to saline. This implies a mix of both aeolian and groundwater salinity influence, largely dependent upon where they are located relative to the CDR. The further points with decreased salinity could be interpreted as beginning to support vegetation from the decreased salinity at a rate fast enough relative to sediment transport, however the aeolian influence still dominates as can be seen from the dune migration rate. Cluster three also shows similar patterns to Cluster two, however dune migration is significantly slower and groundwater salinity is low, in the range of fresh to brackish. Although both factors still influence the dunes it can be interpreted that the groundwater salinity begins to impact migration more at this point in the dune field.

The closeness of the clusters suggests overlapping influence and the need for an increased sample size. The incorporation of the distance to the groundwater table would make for a valuable addition to this analysis. For future studies a more conclusive result could be reached with a multivariate regression, however given the data limitations that approach was not used.

6.4 Parabolic Dunes, Vegetation, and The Groundwater Salinity Gradient

The transition seen in the groundwater salinity gradient underlying the dune field in White Sands National Park is an important component of a dynamic system that is complicated and highly connected to the interactions between vegetation and aeolian forces as they change spatially. Given the findings of this study and those from previous studies, we created an updated conceptual model to help explain these interactions (**Figure 24**).

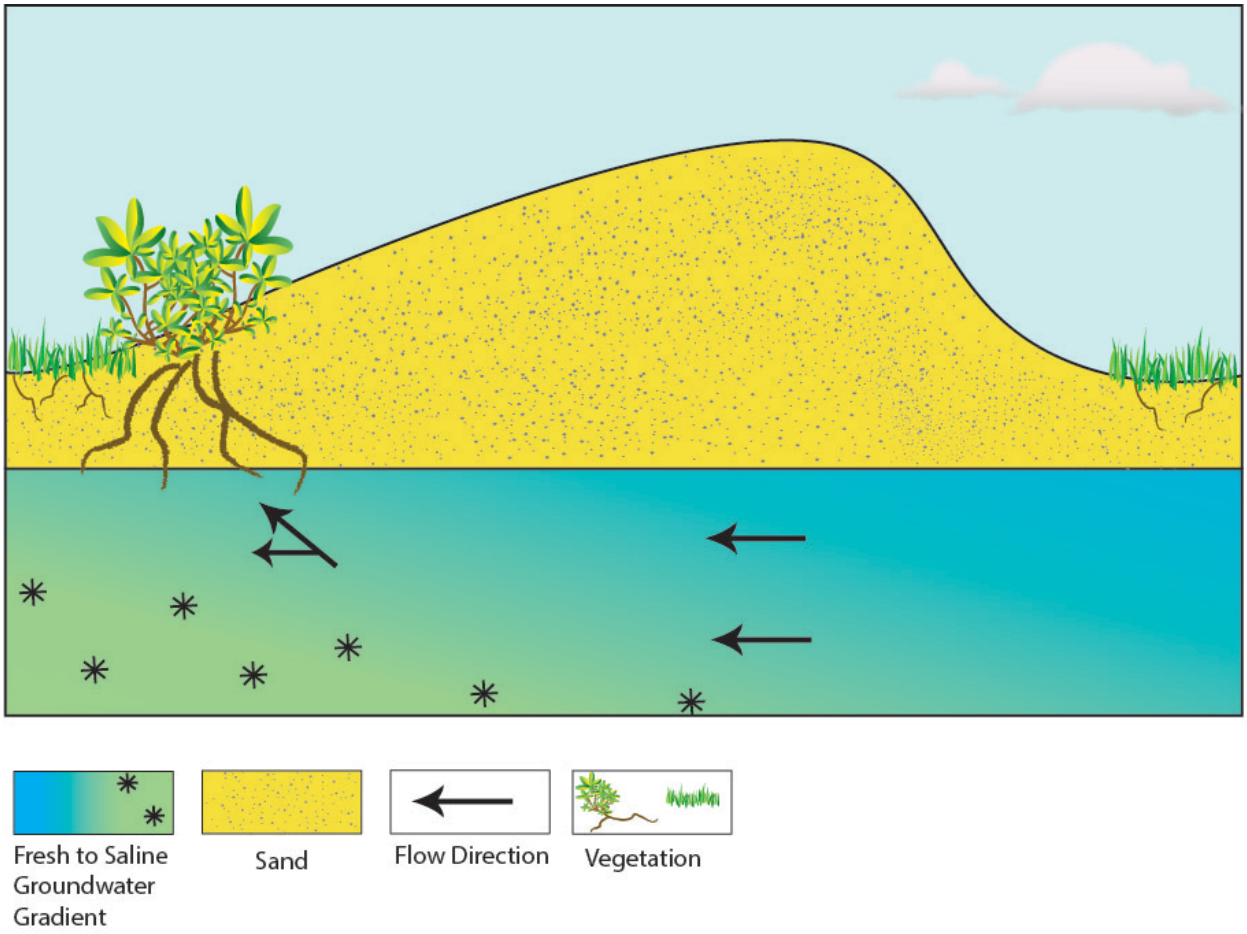

Figure 24. Conceptual model showing the interaction between vegetation and groundwater salinity. As the more highly vegetated parabolic dunes are exposed to freshwater flowing underneath them, the freshwater is slowed from moving down gradient to the west due to vegetations negative pressure created by transpiration. This in turn creates a positive feedback loop in which the freshwater creates a better environment for the vegetation. This increases negative pressure slowing the transport or mixing of the freshwater and making more freshwater available for vegetation to colonize the dunes.

As the highly vegetated parabolic dunes increase in distribution as we move down wind so does the availability of fresh groundwater. The relationship is connected by the vegetation. As the vegetation is able to colonize the dunes it increases the negative pore pressure underneath them by sucking up water. The increased negative pore pressure pulls the freshwater up toward the surface and the plants. The upward pull from the vegetation helps in slowing the diffusion of the freshwater as the underlying regionally saline water moves toward the west.

Additionally, there is a decrease in elevation as the dunes move from east to west forcing diffusion of the freshwater into the saline water and closer to the surface (the freshwater) to evaporate. This decrease in available freshwater, decreases the ability of vegetation to successfully colonize the dunes and thus allows them to remain mobile. Thus, fluctuations in dune field stability are dependent upon the recharge of freshwater during the monsoon season. As freshwater recharge varies from season to season and year to year so does the vegetations ability to survive. Thus, the stability of the parabolic dunes at White Sands is subject to change in fresh groundwater availability due to its impact upon vegetations ability to survive. The separation of the freshwater from the saline groundwater in the eastern margin of the dune field is simultaneously sustained by the vegetations pull upward as long as recharge via precipitation is sufficient.

CHAPTER 7

CONCLUSION

The need to understand freshwater resources has increasingly relevant importance for the sake of our changing world. With a growing population, changing climate, and the pollution of many of our surficial freshwater resources, understanding IFLs and the way they influence their surroundings will allow us to identify and tap into another source of sustainable freshwater. This can help offset the impact of previous generations water resource practices and this generation's increasing demand. IFLs have been previously characterized in other settings but the understanding of their influence upon dune morphology and mobility has not been previously explored in White Sands National Park. This study implemented a first order approach utilizing multiple techniques including remote sensing and a hydrogeologic field investigation to confirm the presence of IFLs in White Sands and understand their impact upon dune field processes. This will give us a better understanding of where else in the world we can expect to find theses formations based on surficial expressions of dune morphology, vegetation, soil moisture, and dune migration rate patterns. It also highlights the need for further data collection and avenues of exploration within this project.

To begin to identify ideal IFL formation settings data collection was the first step before the field study. With limited data sets available online, the WSNP resource manager was able to provide access to several remote sensing data sets including five different years of LIDAR surveys and access to the park's well network and weather station data portal. Additionally, some data was accessed through the NPS data repository, including shapefiles of a vegetation

classification describing dominant species throughout different areas of the park. This allowed for the preliminary implementation of an IO Map highlighting the areas of interest based on characteristics of value that we had access to data on. Due to the groundwater chemistry data quality of the WSNP well network being questionable, trends were also analyzed separately within the LIDAR. Visual trend analysis was performed upon LIDAR difference maps made from surveys of the same transect collected over consecutive years to understand areas of increased mobility. Dune migration rates were calculated via the difference maps. All these factors were considered in conjunction with one another and used to select sites throughout the park to characterize the groundwater table throughout the transect in relation to the surface expression of dune morphology. Sites were selected with the intention of identifying where IFLs were expected to exist as well as where they were not so that comparisons upon surficial settings could be made.

The first objective to identify an IFL was met upon completing the installation of wells, recording in situ groundwater readings, and collecting samples for later analysis. The data supports the existence of a larger regional IFL existing under the eastern section of the dune field under the parabolic section of dunes as well as a localized sub-dune IFL. These findings highlight the need for further investigation to characterize the geometry of the sub-dune IFL and its seasonal extent through the use of more monitoring wells with probes or time-lapse geophysical surveying. The second and third objectives in this study were less conclusive due to limitations of data.

Although there is a statistically significant relationship between the vegetation health and dune mobility, the relationship does not consider the varying effect different vegetation species may have upon dune stability. Similarly, the relationship between groundwater salinity and

vegetation does consider the varying salinity tolerance different species have. Additionally, the resolution at which vegetation health was recorded will likely only recognize reflectance values that the NDVI is calculated from if there is a certain density within each 10 m x 10 m pixel. Further analysis of vegetation recorded over the same transect at higher resolution in conjunction with a more specific vegetation classification could greatly increase the capability of this approach.

The third objective shows that groups did successfully partition based upon the main controlling factor influencing the sampling location, where group one is fully aeolian influenced, group two has coupled control that is dominated by aeolian influence, and group three control is dominated by the presence of freshwater. This interpretation is limited by the sparse amount of data points and the closeness of the clusters. With more data and the implementation of a more complex multivariate regression it would likely characterize both objective two and three more quantitatively.

This study has proven valuable in highlighting gaps of data being recorded in WSNP. The regular recording of LIDAR surveys in conjunction with multispectral data will allow for more in detail analysis of migration patterns in relation to other surficial characteristics. There is also a highlighted need to further characterize the IFLs present within the park to understand their impact upon the ecosystem and determine where else in the world they can form with the growing need for freshwater resources, especially in arid environments.

REFERENCES

Abrams M., Kook S. and Ramachandran B. (2001) ASTER User Handbook Version 2. *ASTER User Handb. Version 2*, 135.

Adams D. C. and Keller G. R. (1994) Crustal structure and basin geometery in south-central New Mexico. In *Basins of the Rio Grande Rift: Structure, Stratigraphy, and Tectonic Setting* (eds. G. R. Keller and S. M. Cather). pp. 241–255.

Allmendinger R. J. (1971) Preliminary evaluation of the role of the hydrologic cycle in the development of the white sands, White Sands National Monument, New Mexico. In *Abstracts with Programs—Geological Society of America* pp. 231–232.

Asghar M. N., Prathapar S. A. and Shafique M. S. (2002) Extracting relatively-fresh groundwater from aquifers underlain by salty groundwater. *Agric. Water Manag.* **52**, 119–137.

Bagnold R. A. (1941) *The Physics of Blown Sand and Desert Dunes*. Reprint 19., Methuen & Company. LTD., London.

Barrett B., Heinson G., Hatch M. and Telfer A. (2002) Geophysical methods in saline groundwater studies: Locating perched water tables and fresh-water lenses. *Explor. Geophys.* **33**, 115–121.

Basabilvazo G. T., Myers R. G. and Nickerson E. L. (1994) *Geohydrology of the High Energy Laser System Test Facility Site, White Sands Missile Range, Tularosa Basin, South-central New Mexico*.,

Bauer K.-H. and Gluhak T. (2019) Ion chromatography in water analysis. *Wiley Anal. Sci. Mag.*

Bauer P., Held R. J., Zimmermann S., Linn F. and Kinzelbach W. (2006) Coupled flow and salinity transport modelling in semi-arid environments: The Shashe River Valley, Botswana. *J. Hydrol.* **316**, 163–183.

Blomqvist G. (1998) *Impact of De-icing Salt on Roadside Vegetation A Literature Review*.,

Borer C. H., Hamby M. N. and Hutchinson L. H. (2012) Plant tolerance of a high calcium environment via foliar partitioning and sequestration. *J. Arid Environ.* **85**, 128–131. Available at: http://dx.doi.org/10.1016/j.jaridenv.2012.06.004.

Bourret S. M. (2015) Stabilization of the White Sands gypsum dune field, New Mexico, by groundwater seepage: A hydrological modeling study. New Mexico Institute of Mining and Technology.

Brod H.-G. (1993) *Langzeitwirkung von Streusalz auf die Umwelt [Bericht zum Forschungsprojekt 9.9125]*.,

Bruckner M. (2021) Ion Chromatography. *Sci. Educ. Resour. Cent. Carlet. Coll.*

Cates D., Knox R. and Sabatini D. (1996) The Impact of Ion Exchange Processes on Subsurface Brine Transport as Observed on Piper Diagrams. *Groundwater1* **34**, 532–544.

Chavdarian G. V. and Sumner D. Y. (2006) Cracks and fins in sulfate sand: Evidence for recent mineral-atmospheric water cycling in Meridiani Planum outcrops? *Geology* **34**, 229–232.

Chongo M., Christiansen A. V., Fiandaca G., Nyambe I. A., Larsen F. and Bauer-Gottwein P. (2015) Mapping localised freshwater anomalies in the brackish paleo-lake sediments of the Machile-Zambezi Basin with transient electromagnetic sounding, geoelectrical imaging and induced polarisation. *J. Appl. Geophys.* **123**, 81–92. Available at: http://dx.doi.org/10.1016/j.jappgeo.2015.10.002.

Coll C., Caselles V., Galve J. M., Valor E., Niclòs R., Sánchez J. M. and Rivas R. (2005) Ground

measurements for the validation of land surface temperatures derived from AATSR and MODIS data. *Remote Sens. Environ.* **97**, 288–300.

Dar I., Qadir J. and Shukla A. (2019) Estimation of LST from multi-sensor thermal remote sensing data and evaluating the influence of sensor characteristics. *Ann. GIS* **25**, 263–281. Available at: https://doi.org/10.1080/19475683.2019.1623318.

Dong P. (2015) Automated measurement of sand dune migration using multi-temporal lidar data and GIS. *Int. J. Remote Sens.* **36**, 5426–5447. Available at: http://dx.doi.org/10.1080/01431161.2015.1093192.

Durán O. and Herrmann H. J. (2006) Vegetation against dune mobility. *Phys. Rev. Lett.* **97**, 1–4.

Elewa H. H. and Qaddah A. A. (2011) Groundwater potentiality mapping in the Sinai Peninsula, Egypt, using remote sensing and GIS-watershed-based modeling. *Hydrogeol. J.* **19**, 613–628.

Engineering Toolbox (2003) Emissivity Coefficient Materials. *Eng. Toolbox*.

Fenton L. K., Bishop J. L., King S., Lafuente B., Horgan B., Bustos D. and Sarrazin P. (2017) Sedimentary differentiation of aeolian grains at the White Sands National Monument, New Mexico, USA. *Aeolian Res.* **26**, 117–136. Available at: http://dx.doi.org/10.1016/j.aeolia.2016.05.001.

Frank A. and Kocurek G. (1994) Effects of atmospheric conditions on wind profiles and aeolian sand transport with an example from white sands national monument. *Earth Surf. Process. Landforms* **19**, 735–745.

Fryberger S. G. (2001) Geological Overview of White Sands National Monument. National Park Service.

Fryberger S. G., Schenk C. J. and Krystinik L. F. (1988) Stokes surfaces and the effects of near-

surface groundwater-table on Aeolian deposition. *Sedimentology* **35**, 21–41. Available at: http://doi.wiley.com/10.1111/j.1365-3091.1988.tb00903.x [Accessed March 4, 2020].

He Q., Silliman B. R. and Cui B. (2017) Incorporating thresholds into understanding salinity tolerance: A study using salt-tolerant plants in salt marshes. *Ecol. Evol.* **7**, 6326–6333.

Houben G., Noell U., Vassolo S., Grissemann C., Geyh M., Stadler S., Dose E. J. and Vera S. (2014) La lentille d'eau douce de Benjamin Aceval, Chaco, Paraguay: un analogue continental des lentilles d'eau douce d'île océanique. *Hydrogeol. J.* **22**, 1935–1952.

Huff G. F. (2005) *Simulation of ground-water flow in the basin-fill aquifer of the Tularosa Basin, south-central New Mexico, predevelopment through 2040*., US Geological Survey.

Huff G. F. (2004) Water Desalination and Reuse Strategies for New Mexico an Overview of the Hydrogeology of Saline Ground Water in New Mexico. , 21–34.

Huff G. F., Sands W., Katherine A., Spencer G., Barry S. and Robert G. (2002) New Mexico Geological Society Basin , Otero County , New Mexico. , 303–307.

Jerolmack D. J., Ewing R. C., Falcini F., Martin R. L., Masteller C., Phillips C., Reitz M. D. and Buynevich I. (2012) Internal boundary layer model for the evolution of desert dune fields. *Nat. Geosci.* **5**, 206–209.

Jerolmack D. J., Reitz M. D. and Martin R. L. (2011) Sorting out abrasion in a gypsum dune field. *J. Geophys. Res. Earth Surf.* **116**, 1–15.

Kacimov A. R. and Obnosov Y. V. (2019) Analytic solutions for fresh groundwater lenses floating on saline water under desert dunes: The Kunin-Van Der Veer legacy revisited. *J. Hydrol.* **574**, 733–743. Available at: https://doi.org/10.1016/j.jhydrol.2019.04.065.

Keller G. R., Morgan P. and Seager W. R. (1990) Crustal structure, gravity anomalies and heat flow in the southern Rio Grande rift and their relationship to extensional tectonics.

Tectonophysics **174**, 21–37.

KellerLyn K. (2012) *White Sands National Monument Geologic Resources Inventory Report*.,

Knight T. M., McCoy M. W., Chase J. M., McCoy K. A. and Holt R. D. (2005) Trophic cascades across ecosystems. *Nature* **437**, 880–883.

Kocurek G., Carr M., Ewing R., Havholm K. G., Nagar Y. C. and Singhvi A. K. (2007) White Sands Dune Field, New Mexico: Age, dune dynamics and recent accumulations. *Sediment. Geol.* **197**, 313–331.

Kocurek G., Mohrig D., Baitis E., Ewing R. C., Smith V. and Peyret A. (2012) LiDAR Surveys of Gypsum Dune Fields in White Sands National Monument , New Mexico.

Kwarteng A. Y., Viswanathan M. N., Al-Senafy M. N. and Rashid T. (2000) Formation of fresh ground-water lenses in northern Kuwait. *J. Arid Environ.* **46**, 137–155.

Laattoe T., Werner A. D., Woods J. A. and Cartwright I. (2017) Terrestrial freshwater lenses: Unexplored subterranean oases. *J. Hydrol.* **553**, 501–507. Available at: http://dx.doi.org/10.1016/j.jhydrol.2017.08.014.

Langford R. P., Rose J. M. and White D. E. (2009) Groundwater salinity as a control on development of eolian landscape: An example from the White Sands of New Mexico. *Geomorphology* **105**, 39–49. Available at: http://dx.doi.org/10.1016/j.geomorph.2008.01.020.

Lee T. M. and Yeh H. C. (2009) Applying remote sensing techniques to monitor shifting wetland vegetation: A case study of Danshui River estuary mangrove communities, Taiwan. *Ecol. Eng.* **35**, 487–496.

Lockwood J. G. (1995) Classics in physical geography revisited. *Prog. Phys. Geogr.* **19**, 243–248.

McKee E. D., Douglass J. R. and Rittenhouse S. (1971) Deformation of lee-side laminae in eolian dunes. *Bull. Geol. Soc. Am.* **82**, 359–378.

McLean J. S. (1970) *Saline Groundwater Resources of the Tularosa Basin, New Mexico*., Available at: http://pubs.er.usgs.gov/publication/70139928.

Metcalfe S. E., O'Hara S. L., Caballero M. and Davies S. J. (2000) Records of Late Pleistocene-Holocene climatic change in Mexico - A review. *Quat. Sci. Rev.* **19**, 699–721.

Milewski A., Sultan M., Al-Dousari A. and Yan E. (2014) Geologic and hydrologic settings for development of freshwater lenses in arid lands. *Hydrol. Process.* **28**, 3185–3194.

Nickling W. G. and Neuman C. M. (2009) *Geomorphology of Desert Environments, Chapter: Aeolian Sediment Transport*.,

Panday S., Huyakorn P. S., Robertson J. B. and McGurk B. (1993) A density-dependent flow and transport analysis of the effects of groundwater development in a freshwater lens of limited areal extent: The Geneva area (Florida, U.S.A.) case study. *J. Contam. Hydrol.* **12**, 329–354.

Parida B. R., Collado W. B., Borah R., Hazarika M. K. and Samarakoon L. (2008) Detecting drought-prone areas of rice agriculture using a MODIS-derived soil moisture index. *GIScience Remote Sens.* **45**, 109–129.

Reitz M. D., Jerolmack D. J., Ewing R. C. and Martin R. L. (2010) Barchan-parabolic dune pattern transition from vegetation stability threshold. *Geophys. Res. Lett.* **37**, 1–5.

Rodríguez-Santalla I., Gomez-Ortiz D., Martín-Crespo T., Sánchez M. J., Montoya-Montes I., Martín-Velázquez S., Barrio F., Serra J., Ramírez-Cuesta J. M. and Gracia F. J. (2021) Study and evolution of the dune field of la banya spit in ebro delta (Spain) using lidar data and gpr. *Remote Sens.* **13**, 1–17.

Rotz R., Milewski A. and Rasmussen T. C. (2020) Transient evolution of inland freshwater lenses: Comparison of numerical and physical experiments. *Water (Switzerland)* **12**.

Rotz R. R. and Milewski A. M. (2019) Physical modeling of inland freshwater lens formation and evolution in drylands. *Hydrogeol. J.*, 1597–1610.

Rouse J. W., Haas R. H., Schell J. A., Deering D. W. and Harlan J. C. (1974) Monitoring the vernal advancements and retrogradation. *Texas, Texas A M Univ.*

Saha A., Patil M., Goyal V. C. and Rathore D. S. (2018) Assessment and Impact of Soil Moisture Index in Agricultural Drought Estimation Using Remote Sensing and GIS Techniques. *Proceedings* **7**, 2.

Scheidt S., Ramsey M. and Lancaster N. (2010) Determining soil moisture and sediment availability at White Sands Dune Field, New Mexico, from apparent thermal inertia data. *J. Geophys. Res. Earth Surf.* **115**, 1–23.

Seager R., Ting M., Held I., Kushnir Y., Lu J., Vecchi G., Huang H.-P., Harnik N., Leetmaa A., Lau N.-C., Li C., Velez J. and Naik N. (2007) Model Projections of an Imminent Transition to a More Arid Climate in Southwestern North America. *Science (80-.).* **316**, 1181–1184. Available at: https://www.jstor.org/stable/20036337.

Slinger D. and Tenison. K. (2007) Salinity Glove Box Guide: Nsw Murray & Murrumbidgee Catchments. Available at: https://www.dpi.nsw.gov.au/agriculture/soils/salinity/general-information/measuring.

Sobrino J. A., Jiménez-Muñoz J. C., Sòria G., Romaguera M., Guanter L., Moreno J., Plaza A. and Martínez P. (2008) Land surface emissivity retrieval from different VNIR and TIR sensors. *IEEE Trans. Geosci. Remote Sens.* **46**, 316–327.

Soininen J., Bartels P., Heino J., Luoto M. and Hillebrand H. (2015) Toward more integrated

ecosystem research in aquatic and terrestrial environments. *Bioscience* **65**, 174–182.

Szynkiewicz A., Ewing R. C., Moore C. H., Glamoclija M., Bustos D. and Pratt L. M. (2010) Origin of terrestrial gypsum dunes-Implications for Martian gypsum-rich dunes of Olympia Undae. *Geomorphology* **121**, 69–83.

Talon B. and Allen N. B. (2014) *Hydrologic Investigation at White Sands National Monument*., Available at: www.geoinfo.nmt.edu [Accessed October 22, 2019].

Xie Y., Sha Z. and Yu M. (2008) Remote sensing imagery in vegetation mapping: a review. *J. Plant Ecol.* **1**, 9–23.